

OPERATING RANGES OF MESOSCALE NUMERICAL MODELS AND METEOROLOGICAL WIND TUNNELS FOR THE SIMULATION OF SEA AND LAND BREEZES

R. AVISSAR¹, M. D. MORAN², G. WU³, R. N. MERONEY³,
and R. A. PIELKE²

¹*Department of Meteorology and Physical Oceanography, Cook College, Rutgers University, New Brunswick, New Jersey, 08903, U.S.A.*

²*Department of Atmospheric Science, Colorado State University, Fort Collins, Colorado, 80523, U.S.A.*

³*Department of Civil Engineering, Colorado State University, Fort Collins, Colorado, 80523, U.S.A.*

(Received 25 May, 1989)

Abstract. The operating ranges of mesoscale numerical models and meteorological wind tunnels for sea- and land-breeze simulations are defined in this paper based on a review of the theoretical and practical limitations of these two approaches. Numerical-model operating ranges are limited by the choice of governing equations, the numerical methods used to solve the governing equations, the scales of the surface or atmospheric forcing and the atmospheric response, the specified grid resolution and domain size, and the available computer resources. Wind-tunnel operating ranges are limited by the dimensions of the simulated circulations and of the tunnel itself, the tunnel flow speed and turbulence characteristics, the temperature gradients within the tunnel, the lack of Coriolis force and moist processes, and the characteristics of the measurement instrumentation. The operating ranges of these two simulation methods are shown to overlap. In this common range, results of simulations from both approaches can be compared so as to strengthen the validity of the results and to help in the development and improvement of parameterizations of physical processes in numerical models. In addition, the coupling of meteorological wind tunnels and mesoscale numerical models offers a larger range of operating conditions than can be achieved by either approach alone. Together, they can be used in a hybrid form to predict atmospheric conditions at the scale of a few meters for complex terrain (e.g., buildings, hills, etc.) within larger mesoscale atmospheric flow regimes. In the case of sea and land breezes, the sea-land transition zone and coastal internal boundary layer can be studied using both approaches.

1. Introduction

Sea breezes and land breezes are terrain-forced, mesoscale atmospheric circulations often observed along the coasts of oceans, lakes, and islands. Although most common in subtropical latitudes, sea breezes have even been observed in the Arctic (e.g., Kozo, 1982). These coastal circulation systems may differ considerably in character from one region to another, varying in direction, intensity, and phase according to local, mesoscale, and synoptic atmospheric conditions, season, coastline shape, coastal topography, and land surface characteristics (e.g., soil texture, soil moisture, vegetation type). The horizontal contrast of surface sensible heat flux between land and water provides the energy needed to drive these mesoscale systems. The prevailing large-scale synoptic pressure pattern also has a direct effect on the strength, persistence, and inland penetration of sea and land breezes (SLBs).

In the absence of significant larger-scale flow, the sea-breeze circulation typically consists of onshore flow less than 1000 m deep at the earth's surface and a weaker but deeper offshore return flow aloft. It develops during the daytime hours and has a maximum intensity during the afternoon. The peak horizontal wind component of the sea breeze is usually in the 5–10 m s⁻¹ range and the maximum vertical component may be anywhere from 0.1 to 7.5 m s⁻¹ (Atkinson, 1981; Wallington, 1961). The land breeze is shallower than the sea breeze and consists of an offshore flow near the earth's surface and an onshore return flow aloft. It is also weaker than the sea breeze because of the increased stratification and reduced turbulent mixing at night (Pearson, 1975; Mak and Walsh, 1976).

These wind systems have long been recognized as important mesoscale perturbations on regional flows and are mentioned in the Old Testament (Ecclesiastes 1:6) and in works by Aristotle and Theophrastus (Neumann, 1973). Given their ubiquity and importance in coastal zones for maritime activities, convection, and pollutant dispersion, it is not surprising that of all the various mesoscale atmospheric phenomena, SLBs appear to have been the most studied, both observationally and theoretically. Reviews of many of these studies may be found in Atkinson (1981), Pielke (1984), and Pielke and Segal (1986).

There are two fundamental methods for simulating SLBs – *mathematical models* and *physical models*. Mathematical models use basic analysis techniques of algebra and calculus to solve the conservation laws of motion, heat, moisture, and other atmospheric constituents either analytically or numerically. In the case of physical models, scale-model replicas of observed ground surface characteristics (e.g., topographic relief, buildings) are constructed and inserted into a controlled-flow laboratory chamber such as a wind tunnel or water channel. The fluid flow through the chamber is adjusted so as to best represent the larger-scale atmospheric flow. Previous applications of these two methods to the study of SLBs are briefly reviewed in the next two subsections.

A. NUMERICAL MODELS OF SEA AND LAND BREEZES

Considerable insight into SLB circulations has been gained from linearized analytical models (e.g., Haurwitz, 1947; Schmidt, 1947; Pierson, 1950; Defant, 1950; Walsh, 1974; Neumann, 1977; Kimura and Eguchi, 1978; Sun and Orlanski, 1981a; Rotunno, 1983; Ueda, 1983; Niino, 1987; and Dalu and Pielke, 1989). However, nonlinear numerical models are usually adopted to simulate complex coastal flows because the full, coupled system of conservation equations is nonlinear and analytically intractable.

A complete numerical treatment of SLBs must consider the pressure gradient force induced by the land–water temperature difference, atmospheric stratification, vertical heat exchange, turbulent friction, the earth's rotation, the prevailing synoptic airflow, and topography. Most early numerical models such as those of Pearce (1955), Estoque (1961, 1962), Fisher (1961), Neumann and Mahrer (1971, 1973, 1974), Walsh (1974), Physick (1976), and Garstang *et al.* (1980a, b) were

two-dimensional and assumed straight coastlines and flat terrain. However, Fosberg and Schroeder (1966), Schroeder *et al.* (1967), Mahrer and Pielke (1977), and Asai and Mitsumoto (1978) all found that the temperature, humidity, and wind patterns associated with the sea breeze are modified extensively as marine air penetrates in and over complex landforms.

McPherson (1970) was the first to examine the effect of a coastal irregularity on the structure of the sea breeze. He integrated a three-dimensional, nonlinear, numerical sea-breeze model which had a large, square bay incorporated into the surface boundary conditions. The presence of the bay produced an asymmetrical distortion of the sea-breeze convergence zone over land, including extrema of vertical motion. This idealized case was extended recently by Itoh and Sugimura (1989).

Pielke (1974a, b) and Pielke and Mahrer (1978) applied a three-dimensional, hydrostatic, mesoscale meteorological model to study sea breezes along the real coastline of southern Florida. Comparison of radar and satellite observations of convective cloud development with model-predicted, low-level convergence zones showed good agreement. Tapp and White (1976) used a three-dimensional, non-hydrostatic mesoscale model in a comparable southern Florida simulation and obtained results similar to those of Pielke. Hsu (1979), Bougeault (1987), and Mahfouf *et al.* (1987) have also simulated this southern Florida case with other three-dimensional, hydrostatic mesoscale models. A discussion and comparison of results from four of these models is given by Arritt (1989).

Sea breezes elsewhere in the world have also been simulated with three-dimensional, prognostic mesoscale models. Warner *et al.* (1978) and Segal *et al.* (1982a) simulated sea breezes in the Chesapeake Bay area of the eastern United States. Other North American cases include the Great Lakes (Lyons *et al.*, 1979; Estoque and Gross, 1981), New York City (Bornstein *et al.*, 1987), the lower British Columbia mainland (Steyn and McKendry, 1988), and the Los Angeles basin (Ulrickson, 1988). Carpenter (1979) and Carpenter and Lowther (1982) have applied Tapp and White's nonhydrostatic model to sea breezes in southern England, while Segal *et al.* (1982b) have modeled sea breezes in the eastern Mediterranean. Sea-breeze circulations in the Kanto district of Japan have been simulated by Kikuchi *et al.* (1981) and Kimura (1985), and Australian sea-breeze cases have been studied by Abbs (1986) and Noonan and Smith (1987). Finally, island sea breezes over Barbados and Sardinia have been simulated by Mahrer and Pielke (1976) and Dalu and Cima (1983), respectively.

Turning to phenomenological studies, McNider *et al.* (1982) have examined some effects of sea-breeze-associated low-level jets which occur in coastal regions when the synoptic conditions drive large-scale flows parallel to the coast. They considered cases both with flat shorelines and with topography using a terrain-following coordinate system in Pielke's mesoscale model. Kikuchi *et al.* (1981), Pielke *et al.* (1983), McNider and Pielke (1984), and Abbs (1986) studied terrain influences on sea breezes, including irregular terrain in coastal or mountain re-

gions. Sun and Orlanski (1981b), Garratt and Physick (1985), Physick and Smith (1985), Noonan and Smith (1986, 1987), and Yan and Anthes (1987) have modeled low-latitude sea breezes, and Abbs (1986) and Noonan and Smith (1986) have considered the interactions of adjacent sea-breeze systems.

Physick (1980) studied the influence of soil moisture on the inland penetration of the sea-breeze front and Segal *et al.* (1986) have evaluated the impact of cloud shading on sea breezes. Recently, Yan and Anthes (1988) investigated the effects of soil moisture variations and Segal *et al.* (1988a) investigated the influence of both vegetation and soil moisture on the development of sea breezes. All of these studies reveal the important influence of the modulation of surface heating over irregular terrain on resultant winds. Kitada *et al.* (1984) considered the transport of reactive pollutants within a SLB system in Japan and Segal *et al.* (1988b) modeled SLB influences on mesoscale pollutant dispersion over the southern Florida peninsula. Stunder and SethuRaman (1985) and Venkatram (1986) reviewed simple models for the development and structure of internal boundary layers in coastal zones. Arritt (1987) examined the influence of water temperature on lake breezes and thermal internal boundary layer (TIBL) development. Durand *et al.* (1989) studied the two-dimensional structure of the TIBL at the Dutch coast using a mesoscale model which employed a third-order turbulence closure scheme. Finally, Arritt (1989) has looked at the influence of latitude, water temperature, atmospheric stratification, gradient wind, and coastal curvature on the offshore extent of sea breezes.

B. PHYSICAL MODELS OF SEA AND LAND BREEZES

Inhomogeneous surface heating of coastlines or hill surfaces is the driving mechanism for SLBs and the anabatic and katabatic winds which may inhibit or enhance airflow over hill crests. Early laboratory work on flow over unevenly heated terrain includes the simulations of urban heat islands by Yamada and Meroney (1971, 1974) and SethuRaman and Cermak (1974, 1975), the simulation of flow and dispersion at shoreline sites by Meroney *et al.* (1975a), and the simulation of dispersion effects of heat given off from large industrial complexes by Meroney *et al.* (1975b).

Meroney *et al.* (1975a) pioneered the use of the wind tunnel as a prediction tool for shoreline air pollution fumigation. They simulated the behavior of plumes emitted from a shoreline fossil fuel power plant near Lake Erie, Ohio. By alternately cooling and heating the test section floor, the shoreline TIBL was reproduced. The growth rate of the TIBL agreed with empirical formulae developed from field data taken at lake and ocean shoreline sites. Ogawa *et al.* (1975) simulated the low-level diffusion patterns associated with sea breezes. No attempt was made to reproduce the recirculation that characterizes a sea breeze (because of wind-tunnel limitations), but their results indicated that the low-level onshore flow was well simulated for neutral, stable, unstable, and elevated inversion con-

ditions. Ogawa *et al.* (1981) briefly discussed results from one sea-breeze simulation made with a new stratified-flow wind tunnel at the Japanese National Institute for Environmental Studies.

Briatore *et al.* (1980) reported on a comparison between local air circulations found over a complex coastal site and corresponding flows in a hydraulic, stratified, laboratory model. The model of the La Spezia gulf area in Italy included shoreline hill barriers within a domain 11 km in diameter at a scale of 1:8,000. Sea-breeze flows were produced by salt solutions injected at the model bottom. The hydraulic model reproduced complicated secondary circulations seen over the bay and the progression of the sea breeze under stationary and transient inversion conditions, and correctly identified regions of maximum velocity. These investigators concluded that the physical modeling technique could reliably be used in planning studies for complex sites, "thus avoiding more expensive and time consuming field observations or making these . . . more simple and reduced".

Mitsumoto *et al.* (1983) used a stratified, temperature-controlled water tank with periodic bottom forcing to simulate a SLB system over a simple straight coastline. Two different flow visualization techniques allowed the characteristics of the coastal circulation to be studied, including cellular convection, longitudinal vortex rows, and propagation of the sea-breeze and land-breeze fronts. Measurements of vertical wind and temperature profiles at different locations in the tank were made with a laser Doppler velocimeter and thermocouple traverses. This simulation was laminar because of the very small velocities, and hence small Reynolds numbers, induced in the tank water. Simpson (1969, 1987) and Simpson and Britter (1979, 1980) have also simulated the propagation of atmospheric gravity currents with water tank models.

C. HYBRID MODELING

Numerical mesoscale models have been quite successful in predicting general wind speed and direction patterns over grid scales of several kilometers or more. Meteorological wind tunnels have accurately reproduced local wind fields down to 10 m horizontal scales but need realistic boundary driving conditions to be most effective. Apparently, the qualities of these two methods have never previously been combined to optimize the description of wind fields or to forecast atmospheric conditions at different scales.

The present paper is the first of a series which will describe our investigations on the coupling of numerical and physical models to simulate SLBs. It reviews the theoretical and practical limitations and operating ranges (ORs) of these two simulation methods and discusses the scales on which they may complement one another to provide a wider modeling OR and the scales on which both techniques are applicable. This common OR can be used to strengthen the simulation results or to validate new developments in numerical modeling.

2. Operating Range for Mesoscale Numerical Models

There are three types of limiting factors inherent in mesoscale atmospheric numerical models. One type of limiting factor arises from the approximations and assumptions made in choosing the form of the mathematical system of equations to be used to describe atmospheric behavior. The second type of limiting factor results from the properties of the numerical scheme used to solve the governing set of simultaneous partial differential equations. The third type depends upon the choice of model grid resolution and model domain size.

A. GOVERNING EQUATIONS

The choice of the mathematical description of a physical system introduces the most fundamental limitations on a numerical simulation of that system. Generally, the governing mathematical equations are tailored to suit the physical system or systems of interest by a judicious choice of simplifications and assumptions. For instance, local time derivatives might be neglected when modeling a steady phenomenon or latent heating could be left out in the simulation of a 'dry' phenomenon. However, such simplifications, assumptions, and approximations may preclude the application of the mathematical model to a different physical system: for instance, clouds or precipitation cannot be treated in a 'dry' model.

A mathematical model may be separated into two constituent parts: model dynamics and model physics. Model dynamics encompass the treatment of fluid motions and forces. Model physics encompass the treatment of physical processes, including sources, sinks, and transport of momentum, heat, and moisture in the model. Aspects of model dynamics important for SLB simulations are time dependence, linearity and horizontal advection, vertical and Coriolis accelerations, and density changes. Physical processes of concern in SLB simulations include radiation, latent heating, surface processes, and turbulent diffusion of heat, moisture, and momentum.

1. *Model Dynamics*

Probably the most basic feature of the SLB circulation system is its diurnal periodicity; in fact, Aristotle, writing in the 4th century B.C., referred to these circulations as 'alternating winds' (Neumann, 1973). Nevertheless, in what may have been the first quantitative SLB model, Jeffreys (1922) chose to ignore local time derivatives of the wind and assumed a steady state. He also ignored the Coriolis force and classified SLBs as antitriptic winds, i.e., winds in which the pressure gradient force is primarily balanced by frictional forces. Despite the simplicity of his model, Jeffreys was still able to obtain quite reasonable values for sea-breeze wind speed and depth. All subsequent sea-breeze models have included at least some of the local time derivatives.

As mentioned in the Introduction, linearized analytical models have advanced our understanding of SLB circulations considerably. Neglect of the advection

terms due to linearization still permits qualitatively reasonable predictions of many aspects of SLB structure and behavior (e.g., Atkinson, 1981). However, the SLB circulation does modify the temperature field which provides its driving force, resulting in a feedback loop between the velocity and temperature fields. In the onshore flow of a sea breeze, horizontal advection enhances mass convergence over the heated land surface, thereby tightening the horizontal pressure gradient. The increased pressure gradient in turn drives additional convergence due to horizontal advection, and this positive feedback continues until frictional retardation restores a balance (Martin and Pielke, 1983). Inclusion of the nonlinear advection terms will also shift the maximum horizontal wind speed inland and increase the updraft velocities associated with the intruding sea-breeze front (Walsh, 1974; Kimura and Eguchi, 1978). However, the main impact of nonlinear advection is the decrease in the horizontal spatial scale of the SLB circulation (i.e., the atmospheric response) from that of the forcing (Pielke, 1984, p. 338). This scale reduction is an important consideration in the choice of grid resolution for a nonlinear numerical model. In addition, it is nonlinear wave-wave interactions which produce the downscale turbulent cascade of kinetic energy from the generating scales through the inertial range to the dissipating molecular scales. This important process also requires inclusion of the nonlinear terms.

Another important aspect of mesoscale model dynamics is the treatment of vertical accelerations. Atmospheric models which assume that the acceleration term in the vertical momentum equation is much smaller than the pressure gradient and buoyancy terms and can be neglected are called hydrostatic. Atmospheric models which retain this vertical acceleration term are called nonhydrostatic. Scaling arguments suggest that vertical accelerations can safely be neglected relative to the vertical pressure gradient force when the horizontal scale of the phenomenon of interest is of the same order or greater than the density scale depth of the atmosphere, about 8 km (Pielke, 1984, p. 33). In the case of SLB circulations, the majority of numerical modelers have used the hydrostatic approximation (e.g., Pielke, 1974a; Walsh, 1974; Warner *et al.*, 1978). Martin and Pielke (1983) have examined the validity of this approximation for SLB simulations in considerable detail. They conclude that scales of heating and cooling as small as 6 km may be handled by hydrostatic models for SLB simulations over flat terrain. On the other hand, if there is a need to simulate the sea-breeze front (i.e., the leading edge of the onshore marine flow) accurately, a nonhydrostatic model will be required since the sea-breeze front often has an intense ($1-7 \text{ m s}^{-1}$), narrow (150–200 m) updraft embedded within a 1–3 km wide convergence zone (Wallington, 1959, 1961, 1965; Findlater, 1964; Simpson, 1967; Lyons, 1972; Simpson *et al.*, 1977; Helmis *et al.*, 1987). Use of the hydrostatic assumption will also remove sound waves as possible solutions to the governing equations, modify the phase speed and direction of internal gravity waves, and eliminate the possibility of gravity wave ‘trapping’ or ‘ducting’ when the atmospheric lapse rate is not uniform (Tapp and White, 1976; Smith, 1979; Pielke, 1984).

Since the earth is a rotating body, a reference frame fixed relative to the earth's surface will be noninertial. Thus, the equations of motion require inclusion of a Coriolis force or acceleration term to obtain an inertial, non-rotating reference frame. The dimensionless Rossby or Kibel number is defined as $Ro = U_0/fL_0$, where U_0 is the advective velocity scale, f is the Coriolis parameter, and L_0 is a characteristic horizontal length scale. The Rossby number arises from scale analysis of the horizontal momentum equations as the ratio of the advective terms to the Coriolis term. If $Ro \gg 1$, as on the cloud scale ($L_0 < 20$ km), the Coriolis acceleration may be neglected relative to the advective terms. If $Ro \ll 1$, as on extratropical cyclone and planetary wave scales ($L_0 > 2000$ km), the Coriolis acceleration dominates the advective terms and the flow of interest will be quasi-geostrophic, that is, constrained by the gradient wind relation. On intermediate scales such as the SLB scale, the Coriolis term will be significant but not dominant. Although late nineteenth century observations of SLB circulations mentioned the horizontal 'rotation' of the wind over the course of a day (Atkinson, 1981), analytical models of the SLB circulation did not include Coriolis acceleration until the work of Haurwitz (1947) and Schmidt (1947). The most important role played by the Coriolis force in SLB circulations is its control of the horizontal scale of the circulation (e.g., Rotunno, 1983; Niino, 1987; Dalu and Pielke, 1989). The rate of local turning of the sea and land breezes is not uniform since it is determined both by the Coriolis effect and by other factors (Neumann, 1977, 1984; Kusada and Alpert, 1983).

The mass continuity equation plays an important role in mesoscale models. In hydrostatic models, the vertical velocity component is often directly diagnosed from this equation. In nonhydrostatic models, the mass continuity equation is needed to calculate the mesoscale perturbation pressure. Mesoscale atmospheric modelers have a choice of three forms of the mass continuity equation: the incompressible form, the anelastic form, or the fully compressible form (Pielke, 1984). The simplest of these three, the incompressible continuity equation, is quite accurate for shallow circulations (that is, circulations whose vertical scale is considerably less than the atmospheric density scale depth of 8 km) but is unsuitable for deeper circulations. In addition, the incompressibility assumption eliminates sound waves as a possible solution. The anelastic continuity equation, so called because it also does not admit sound waves as a solution, does include vertical variations of density so that it can be applied to deep atmospheric circulations (e.g., Ogura and Phillips, 1962; Durran, 1989). The anelastic continuity equation, like the incompressible continuity equation, is a diagnostic equation. The third form of the continuity equation, the time-dependent compressible continuity equation, is a prognostic equation for density and does admit sound waves as possible solutions. Despite the apparently greater complexity of the compressible continuity equation compared to the anelastic equation, the computational complexity of the two can be comparable (e.g., Klemp and Wilhelmson, 1978; Cotton

and Tripoli, 1978). Since SLBs are shallow phenomena, any of the three forms of the continuity equation may be employed.

2. Model Physics

Radiative processes are fundamental to SLB circulations since the daytime heating and nighttime cooling of the coastal zone drive the circulation. Thus, radiative processes must be included in a numerical model if the surface forcing is to be represented correctly. Radiative interactions with clouds may also be important if moist processes are also included in the model (e.g., Stephens, 1984; Segal *et al.*, 1986).

Surface processes are obviously fundamental to SLBs because these circulations are driven by differential or inhomogeneous surface heating. All analytical SLB models and early numerical SLB models specified surface temperatures or heat fluxes. Physick (1976) developed the first numerical mesoscale model in which surface temperature was predicted, thus permitting feedbacks between atmosphere and earth. He used a heat budget technique for the earth's surface and a multi-level soil model. An alternative method is to use a single-layer soil 'slab' model (Blackadar, 1977). Additional realism is obtained if soil moisture and vegetation effects are considered. Both of these factors determine the partitioning between sensible and latent surface energy fluxes (i.e., the Bowen ratio) and affect the surface albedo. Efforts to include these effects in mesoscale models have been made by Deardorff (1978), Physick (1980), McCumber and Pielke (1981), Mahfouf *et al.* (1987), Segal *et al.* (1988a), and Avissar and Pielke (1989), among others.

In a SLB circulation in the absence of significant synoptic flow, moist marine air will be advected onshore during the day and drier continental air will move offshore at night, resulting in the modification of vertical stability and surface fluxes of heat and moisture due to horizontal advection. Shallow cumulus clouds may also form at the top of the daytime convective boundary layer and deep convection may be triggered by rising motion at the sea-breeze front when the atmosphere is convectively unstable. Several treatments of moisture and moist processes are used in mesoscale models. Levels of moisture parameterization include no moisture, water vapor only, stable precipitation (i.e., grid-resolvable clouds and precipitation), cumulus parameterization, and explicit microphysics (e.g., Cotton and Anthes, 1989; Zhang *et al.*, 1988). Moist processes have been neglected in most SLB simulations to date but should be included if the deep convection and precipitation sometimes associated with SLB circulations are to be modeled.

Finally, the turbulent diffusion of momentum, moisture, and particularly heat are important physical processes which need to be considered in any realistic SLB model. Pearson (1975) and Mak and Walsh (1976) have suggested that static stability and eddy diffusivities determine SLB depths and intensities and can explain the observed difference in the intensity of land breezes and sea breezes.

Many hundreds of papers have been written on the parameterization of turbulent diffusion in the planetary boundary layer. From the point of view of the governing equations, however, the most important aspect of the transport of various quantities by a spectrum of turbulent eddies coupled through the nonlinearity of the equations of motion is that all scales are dynamically important. The challenge of dealing with this wide range of motions down to the dissipative eddies on the Kolmogorov microscale is overwhelming.

In order to make the problem more manageable, spatial and temporal scales are specified for the conservative equations. That is, the governing equations are averaged in some fashion, and the flow field is divided into resolved motions and unresolved 'turbulent' motions. Turbulent effects such as Reynolds stresses must then be parameterized as functions of the larger-scale resolved flow. Two main types of averaging have been employed: 'top-hat' averaging and Reynolds averaging. Reynolds averaging is further distinguished by the choice of averaging operator: an ensemble average or a grid-volume average. Most mesoscale models use ensemble-average turbulence parameterizations. More recently, smaller-scale large-eddy simulation models have been developed which use a grid-volume-average approach and explicitly resolve the largest, energy-containing eddies (although an ensemble-average scheme is still used for the subgrid-scale parameterization). Much more detail on these topics may be found in Wyngaard (1982), Pielke (1984), and Cotton (1986).

B. NUMERICAL SCHEMES

There are several broad classes of solution techniques available to represent terms involving spatial derivatives in the governing partial differential equations, including finite-difference schemes, spectral and pseudospectral schemes, finite-element schemes, and interpolation schemes.

In mesoscale atmospheric models, only the finite-difference, finite element, and interpolation schemes have generally been used. Although the spectral and the pseudospectral techniques have been shown to be highly accurate (e.g., Gottlieb and Orszag, 1977; Merilees and Orszag, 1979), the mathematical expressions which result from the Fourier transformation are cumbersome to handle and require periodic boundary conditions to work effectively. Thus, these two techniques have not found wide acceptance among mesoscale atmospheric modelers.

Since the purpose of this section is to describe the limitations on mesoscale numerical model ORs due to model numerics, only some of the simpler numerical schemes will be discussed here because of their amenability to analysis. The more sophisticated numerical solution techniques commonly used in mesoscale models may perform better than the simpler schemes but will still suffer from at least some of the same problems discussed here: phase errors, amplitude errors, aliasing, numerical instabilities, and computational modes. More detailed discussions of numerical schemes are given by Mesinger and Arakawa (1976), Haltiner and

Williams (1980), Long and Pepper (1981), Pielke (1984), Rood (1987), and Tremback *et al.* (1987), among many others.

1. Advection

The advection terms in the conservation equations can be written in the form

$$\frac{\partial \bar{\phi}}{\partial t} = -\bar{u}_j \frac{\partial \bar{\phi}}{\partial x_j}, \quad (1)$$

where $\bar{\phi}$ refers to any one of the dependent variables and \bar{u}_j is the resolved wind velocity component in the x_j direction. The overbar symbol denotes an averaging operator as discussed in the previous section.

The errors introduced by a numerical scheme in representing these terms results from the ability, or lack thereof, of the numerical scheme to (i) conserve the exact amplitude and (ii) preserve the proper phase of different wavelengths.

Probably the simplest advection scheme which has been used in numerical models is the forward-in-time, linear-interpolation upstream scheme. Using this scheme, Equation (1) is approximated by the finite difference equations

$$\bar{\phi}_i^{\tau+1} = \begin{cases} \bar{\phi}_i^\tau - C(\bar{\phi}_{i+1}^\tau - \bar{\phi}_i^\tau), & \bar{u}_{ij} \leq 0, \\ \bar{\phi}_i^\tau - C(\bar{\phi}_i^\tau - \bar{\phi}_{i-1}^\tau), & \bar{u}_{ij} > 0, \end{cases} \quad (2)$$

where $C = \bar{u}_{ij}\Delta t/\Delta x_j$ is the Courant number, τ and $\tau + 1$ are consecutive time levels, Δt is the time step, Δx_j is the grid interval in the j -direction, $i - 1$, i , and $i + 1$ denote three consecutive grid points along the j -axis, and \bar{u}_{ij} is the velocity component value in the j -direction at the i -th point.

Figure 1 portrays the 'numerical web' of this scheme, a graphical illustration of this advection scheme's wave damping and phase conservation properties. Wave damping (ordinate axis) is expressed by the ratio of the computational amplitude change λ_c (from Equation (2)) to the analytical amplitude change λ_a (from Equation (1)) of the solution per time step. (Note that λ_a is unity for this case). Phase conservation (abscissa) is expressed by the ratio of the computational phase speed $c_{\bar{\phi}}$ to the true solution phase speed U . The exact solution of the linear advection equation is represented by the intersection of the $\lambda_c/\lambda_a = 1$ and $c_{\bar{\phi}}/U = 1$ lines. Therefore, the reliability of the numerical scheme is characterized schematically by the convergence of the different wavelengths ($n\Delta x$) at different Courant numbers to the point ($\lambda_c/\lambda_a = 1$, $c_{\bar{\phi}}/U = 1$) at the center of the web. If $\lambda_c/\lambda_a > 1$ for any resolvable wavelength, then the solution is linearly unstable; if $\lambda_c/\lambda_a < 1$ for all resolvable wavelengths, then the scheme is damping. For the forward-in-time, linear-interpolation upstream scheme, the damping is stronger for short wavelengths at all Courant numbers, with maximum damping at $C = 0.5$ and no damping at $C = 0.0$ and $C = 1.0$. Complete damping ($\lambda_c/\lambda_a = 0$) occurs for a $2\Delta x$ wave at $C = 0.5$.

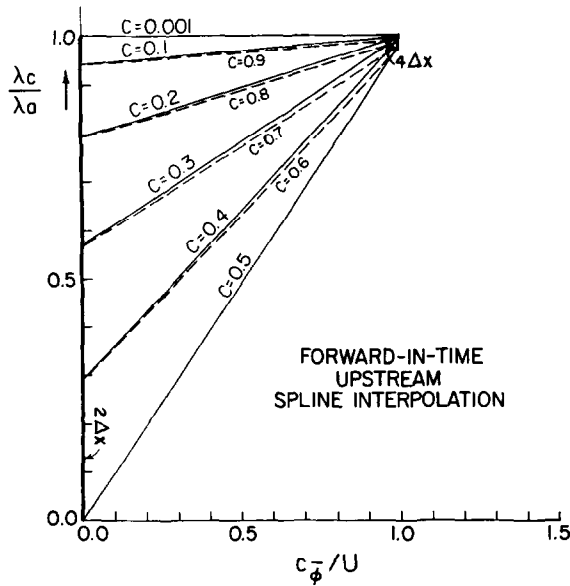


Fig. 2. Same as Figure 1 but for cubic spline interpolation scheme.

implicit (see next section) finite element scheme with equal weighting of present and future values, the phase speed is computed quite accurately for all wavelengths except the $2\Delta x$ waves, which are stationary ($c_{\bar{\phi}}/U = 0$) for all Courant numbers (Figure 3). The phase speed of $4\Delta x$ or longer waves is less accurate for larger Courant numbers, but even with C as large as 2.0, $c_{\bar{\phi}}/U = 0.625$ for $4\Delta x$ waves and $c_{\bar{\phi}}/U = 0.968$ for $20\Delta x$ waves. For the case of the leapfrog scheme, the accuracy of the phase representation deteriorates markedly for the shorter wavelengths at low Courant numbers (Figure 4). The $2\Delta x$ waves are also stationary for this scheme. However, because of the quadratic form of the adjective terms for this scheme (e.g., Pielke, 1984, p. 283), two wave solutions are obtained. One moves downstream ($c_{\bar{\phi}} > 0$ when $U > 0$) and is related to the real solution of the advection equation. The other moves upstream and is called the computational mode. Such separation of solutions can be controlled by occasionally averaging in time to assure that the even and odd time steps remain consistent with one another (e.g., Mesinger and Arakawa, 1976).

2. Diffusion

Subgrid-scale correlation terms such as Reynolds stress terms can be represented as the product of an exchange coefficient (K) and the gradient of the appropriate dependent variable (first-order closure). When the exchange coefficient is assumed constant, the diffusion equation is written as

$$\frac{\partial \bar{\phi}}{\partial t} = K_j \frac{\partial^2 \bar{\phi}}{\partial x_j^2}, \tag{3}$$

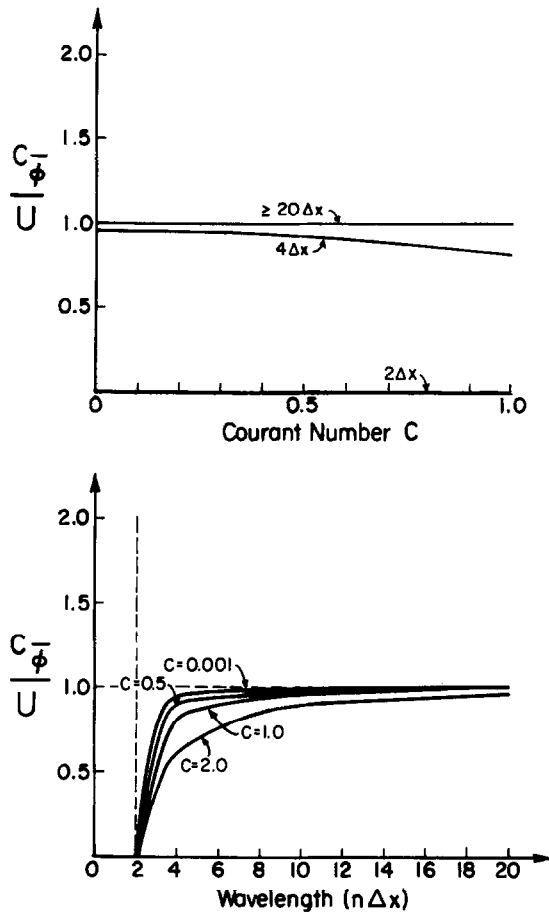


Fig. 3. The relation between the phase-speed ratio of the computational solution to the analytical solution of the linear advection equation (c_ϕ/U) and (a) Courant number (C) and (b) wavelength ($n\Delta x$) for the implicit finite-element advection scheme with chapeau basis function and equal weighting of present and future values (based on Table 10.1 of Pielke, 1984).

where K_j is the eddy exchange coefficient in the j direction. The explicit representation of this equation as a forward-in-time, centered-in-space finite difference expression is

$$\bar{\phi}_i^{t+1} = \bar{\phi}_i^t + \gamma(\bar{\phi}_{i+1}^t - 2\bar{\phi}_i^t + \bar{\phi}_{i-1}^t), \tag{4}$$

where $\gamma = K_j \Delta t / (\Delta x_j)^2$ is called the Fourier number.

Figure 5 shows the influence of the Fourier number and the wavelength on the ratio of the amplitudes of wave solutions to Equations (3) and (4). While long waves (wavelengths $\geq 10\Delta x$) are handled well by the diffusion operator represented with this scheme, shorter waves are strongly disturbed: $2\Delta x$ waves are damped too quickly by diffusion in the numerical solution as compared to the analytical solution for Fourier numbers less than 0.2; $4\Delta x$ waves are not damped enough

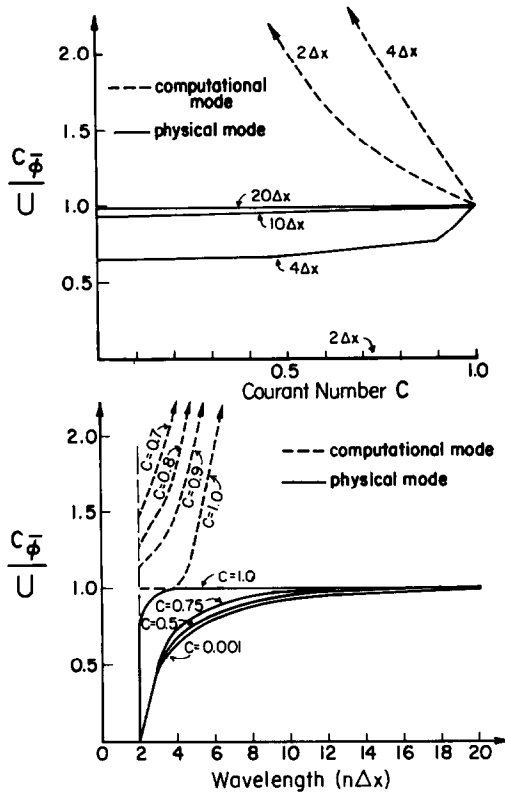


Fig. 4. Same as Figure 3 but for the leapfrog scheme.

and at $\gamma = 0.5$ are not damped at all. For $\gamma > 0.5$, this scheme is linearly unstable.

Implicit schemes, in contrast to explicit schemes which use only the value of the dependent variable at the current time step, also use information from the future time step. A weighting factor $0 \leq \beta \leq 1$ is defined to express the relative weights of the contributions of the future and current time levels to the numerical approximation of the diffusion equation. For $\beta = 1$, the explicit scheme is obtained. In general, the use of an implicit scheme permits use of larger Fourier numbers, that is, longer time steps, than does the explicit scheme without causing linear instability.

Figures 6 and 7 demonstrate the influence of Fourier number and wavelength on the amplitude damping of wave solutions for values of β of 0.7, 0.5, 0.3 and 0.1, respectively. Like the explicit scheme ($\beta = 1.0$; Figure 5), long waves are not affected by the Fourier number value at the different values of β presented here. However, the combination of high Fourier number values and low values of β results in a much too weak damping of shorter waves. For large values of β , the implicit schemes tend to behave like the explicit scheme.

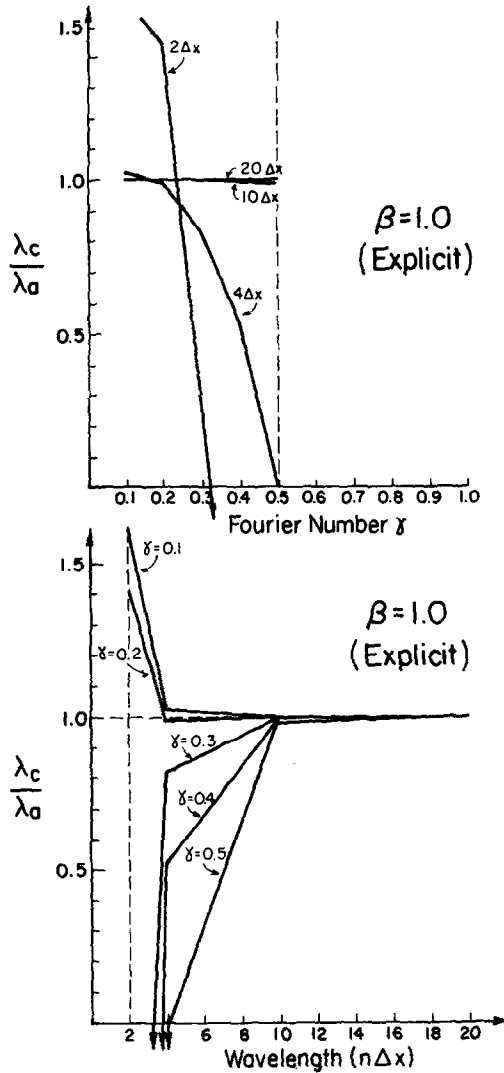


Fig. 5. The relation between the amplitude ratio of the computational solution to the analytical solution of the diffusion equation and (a) Fourier number (γ) for four different wavelengths, $2\Delta x$, $4\Delta x$, $10\Delta x$ and $20\Delta x$, and (b) wavelength ($n\Delta x$) for five different Fourier numbers, $\gamma = 0.1, 0.2, 0.3, 0.4$, and 0.5 , of explicit diffusion scheme (time-level weighting factor $\beta = 1.0$ based on Table 10.2 of Pielke, 1984).

3. Filtering

Nonlinear wave-wave interactions may transfer energy to shorter wavelengths than can be resolved by a numerical model for a chosen grid. When this occurs, the energy is not lost, but rather is projected erroneously onto a resolvable wavelength. Such spatial *aliasing* or *folding* is analogous to the time aliasing about the Nyquist frequency which occurs in time series analysis. One effect of aliasing in a mesoscale

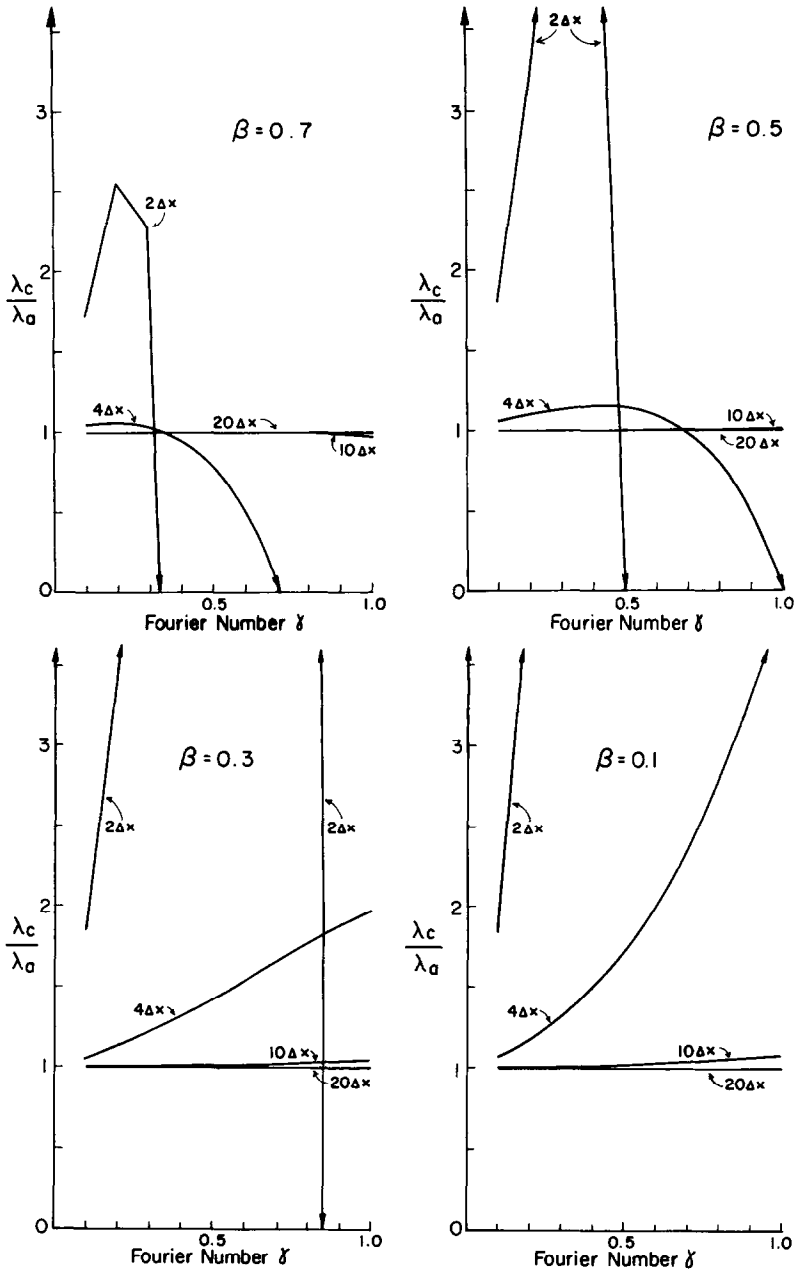


Fig. 6. Same as Figure 5a but for the implicit scheme with time-level weighting factor values of (a) $\beta = 0.7$, (b) $\beta = 0.5$, (c) $\beta = 0.3$, and (d) $\beta = 0.1$.

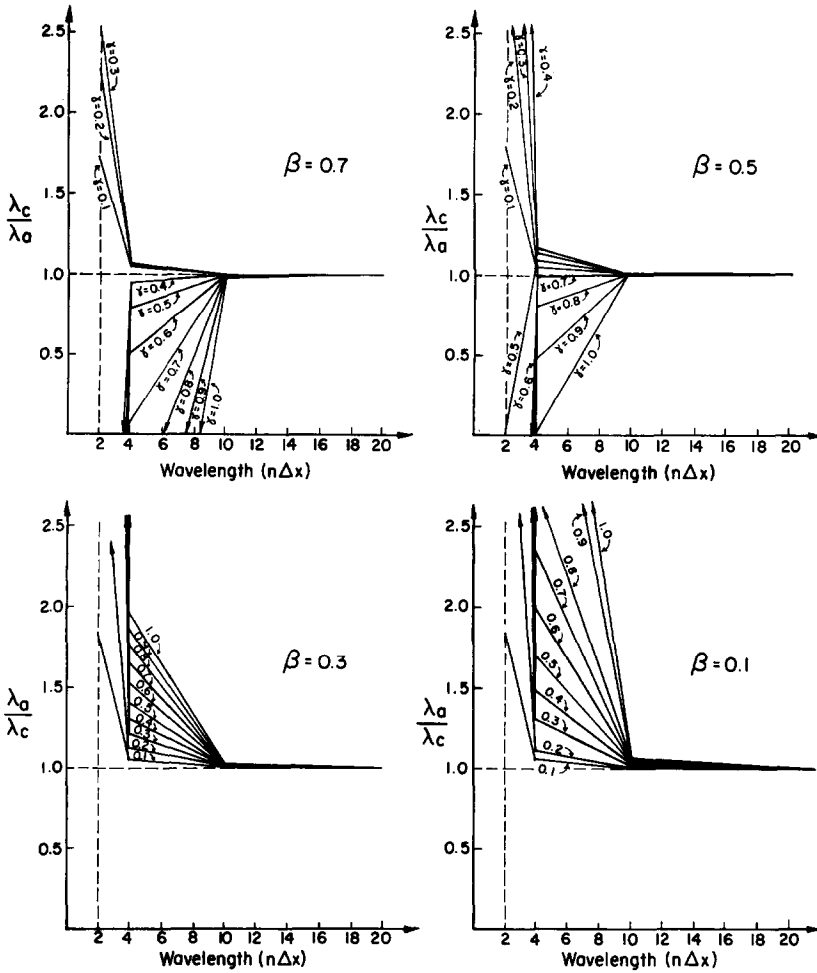


Fig. 7. Same as Figure 5b but for ten Fourier numbers, $\gamma = 0.1, 0.2, \dots, 0.9, 1.0$, and the implicit scheme with time-level weighting factor values of (a) $\beta = 0.7$, (b) $\beta = 0.5$, (c) $\beta = 0.3$, and (d) $\beta = 0.1$.

model is the interruption of the turbulent cascade of energy towards small scales, sometimes resulting in a degradation of model results into physically meaningless computational noise and sometimes even in an unbounded accumulation of energy at the shortest wavelengths, a computational error known as nonlinear stability (e.g., Mesinger and Arakawa, 1976, p. 37). Wavelengths shorter than $4\Delta x$ are required for aliasing to occur. As already discussed, such short wavelengths are badly handled by various numerical schemes even for linear scalar advection. The solution adopted of necessity by modelers has been to ‘control’ the shortest wavelengths by using some sort of spatial smoother or filter to damp or even remove these waves. One way to do this is to include nonphysical horizontal diffusion terms in the governing equations. This makes use of the damping proper-

ties of diffusion to control nonlinear aliasing by damping the shortest wavelengths (e.g., Haltiner and Williams, 1980, p. 155).

An alternative to introducing a nonphysical diffusion term is to apply a selective spatial filter which will damp wavelengths smaller than $4\Delta x$ each time step but which does not affect larger waves (e.g., Purser, 1987; Raymond, 1988). One spatial filter which has been used in mesoscale numerical modeling was suggested by Pepper *et al.* (1979). It has the form

$$(1 - \delta)\phi_{i+1}^* + 2(1 + \delta)\phi_i^* + (1 - \delta)\phi_{i-1}^* = \phi_{i+1} + 2\phi_i + \phi_{i-1}, \quad (5)$$

where ϕ and ϕ^* are the dependent variable to be smoothed and the smoothed value, respectively, and δ is an arbitrarily chosen weighting parameter or filter coefficient for the smoothed value with range $0 \leq \delta \leq 1$. Figure 8 shows the influence of δ on the amplitude of different wavelengths. This filter eliminates $2\Delta x$ waves at each application (provided that cyclic boundary conditions are used and filtering is only in one direction), and its smoothing of longer waves is dependent on the value of δ . For $\delta = 1.0$, the highest filter value, $4\Delta x$ waves are damped by 50% but long waves (wavelengths $\geq 20\Delta x$) are almost unaffected. For $\delta = 0.001$, only $2\Delta x$ waves are damped significantly. Note that in some cases, it may also be necessary to employ a time or frequency filter (e.g., Mesinger and Arakawa, 1976; Haltiner and Williams, 1980).

c. GRID RESOLUTION AND DOMAIN SIZE

The selection of the grid resolution and the domain size in a mesoscale model is dictated by (i) the size and dimensionality of the forcing, (ii) the spatial scales of the atmospheric response to this forcing, and (iii) the available computer resources.

1. Grid Resolution

The grid resolution or spacing used in a mesoscale numerical model depends upon the spatial extent of the atmospheric features of interest. As just discussed, the smallest feature of interest needs to be represented by at least four grid increments due to the fact that numerical schemes tend not to represent shorter wavelengths very well. Hjelmfelt and Braham (1983) simulated lake-effect snowstorms over Lake Michigan, a large lake approximately 120 km wide, and varied the grid resolution in their mesoscale numerical model. Their study suggested that a horizontal grid size larger than 20 km is insufficient to resolve the observed lake-effect snow events. In the case of terrain-forced mesoscale circulations such as SLBs, it is also important to resolve significant terrain features. In complex terrain, it is not always clear by inspection what spatial resolution is required. Young and Pielke (1983), Young *et al.* (1984), and Steyn and Ayotte (1985) have discussed the spectral analysis of terrain irregularities in detail.

Resolving the forcing may not be enough. If the conservation relations were linear, the spatial scale of the forcing would equal the spatial scale of the response.

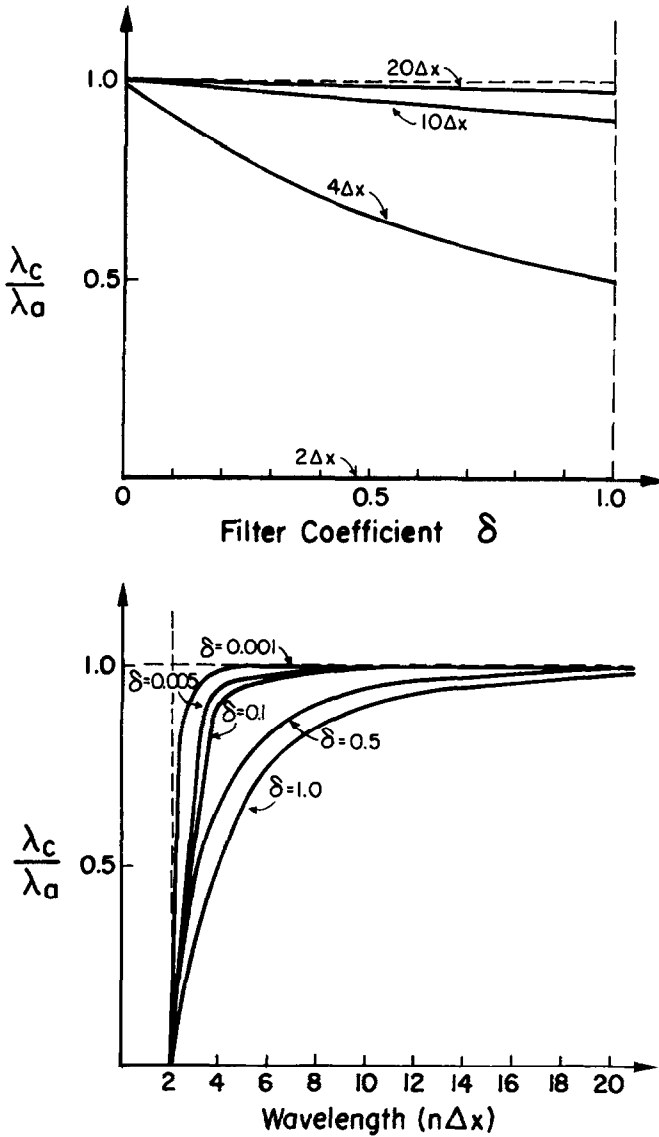


Fig. 8. The relation between the amplitude ratio of the filtered solution to the unfiltered solution (λ_c/λ_a) and (a) filter coefficient (δ) and (b) wavelength ($n\Delta x$) for the Pepper *et al.* (1979) filter.

However, the nonlinearity of the conservation relations acts to decrease the minimum horizontal spatial scale of the response compared to the scale of the forcing. In practice, the only way to ensure that all significant spatial scales are simulated in a nonlinear model is to perform integrations with progressively finer resolution. When the results do not change significantly for a given scale of forcing with further reduction of the grid spacing, sufficient spatial resolution has been achieved.

The choice of grid resolution must also be compatible with the assumptions

made in choosing the governing equations. For instance, Martin and Pielke (1983) have shown with a linear model that the minimum horizontal scale of surface forcing which allows the application of the hydrostatic assumption in mesoscale models is dependent on the atmospheric stability. Under unstable conditions, this minimum scale is about 10 km while under stable conditions, the minimum scale may be as low as 1 km. In the case of a small feature of interest, the need to choose a small enough grid spacing to resolve the feature adequately may conflict with the need to choose a large enough grid spacing to satisfy the hydrostatic assumption.

2. Domain Size

Choice of domain size for a mesoscale numerical model is affected by a number of conflicting constraints. The primary constraint is obvious – the model domain must be large enough to contain the mesoscale circulation feature of interest. Extratropical sea breezes tend to penetrate 20–50 km inland and may extend 100 km or so seaward (Atkinson, 1981). Thus, the model domain should be at least 200 km in extent for an SLB simulation. However, the horizontal extent of the sea breeze appears to be governed by a modified Rossby radius of deformation, $Nh(f^2 + \lambda^2 - \omega^2)^{-1/2}$, where N is the Brunt–Väisälä frequency, h is the SLB depth, λ^{-1} is the damping time due to friction, and ω is the diurnal frequency (Rotunno, 1983; Dalu and Pielke, 1989). Tropical sea breezes thus penetrate farther inland and extend farther seaward so that larger domains are required for low-latitude SLB simulations (e.g., Garratt and Physick, 1985; Yan and Anthes, 1987; Arritt, 1989).

Where possible, many mesoscale models ignore horizontal spatial variations in the background synoptic environment. That is, wind fields, temperature fields, and so on are assumed to be horizontally homogeneous except for mesoscale perturbations such as SLBs driven by terrain forcing. However, at larger scales, horizontal variations in atmospheric fields associated with transient extratropical cyclones and anticyclones cannot be ignored. The assumption of horizontal homogeneity will normally be unreasonable for domain scales larger than 1000 km, thus imposing an upper bound on the choice of domain size. Domain-scale horizontal inhomogeneities can be dealt with but require more complex treatments of model initial fields and lateral boundary conditions (e.g., Haltiner and Williams, 1980; Pielke, 1984).

When discussing model domain size, we should also mention a fourth dimension, time. Since we would like the domain to encompass the entire phenomenon of interest, we should run the model long enough to simulate the full phenomenon life cycle. In the case of a SLB circulation, the model should be run for at least one complete diurnal cycle. In addition, most numerical models require some ‘spin-up’ time at the beginning of the simulation to allow the specified initial fields to come into balance. This initialization component of the simulation may require a sizable fraction of the total simulation run time in some cases. Mesoscale model

initialization techniques include objective analysis, dynamic initialization, and normal mode initialization (e.g., Anthes, 1983; Pielke, 1984). Furthermore, if the synoptic-scale environment outside of the model simulation domain changes with time over the simulation period, then the lateral and upper boundary conditions will have to be constructed so as to feed these changes to the model.

In order to reduce the number of grid points required in a numerical simulation, and hence the computational costs, the modeler would also like to make his domain as small as possible as well as using as coarse a grid resolution as possible. However, Anthes and Warner (1978) and Pielke (1987) have demonstrated that a horizontal domain size of at least 10 km is required in mesoscale numerical models due to the domain-scale accelerations which result from even minimal pressure gradient errors at the lateral boundaries. The spatial extent of the forcing and of the resultant perturbation fields also imposes another lower bound on the choice of domain size for the model.

Another constraint working against the minimization of domain size is the problem of contamination of the solution by noise or reflections from the lateral boundaries. The specification of lateral boundary conditions in a limited-area model has bedevilled modelers for decades. Several approaches have been tried, but none has proven completely satisfactory. A rule of thumb is to keep the simulated feature of interest as far from the model boundaries as possible, which implies use of as large a domain as possible. Stretched grid coordinates and nested grids are two approaches which have been proposed to deal with the modeler's desire for both detailed grid resolution and large domain size (e.g., Clark and Farley, 1984; Pielke, 1984; Zhang *et al.*, 1986).

D. NUMERICAL-MODEL OPERATING RANGE (OR) FOR SLB SIMULATIONS

The three types of limiting factors just discussed all constrain the numerical-model operating range (OR). Figure 9 shows the OR of mesoscale numerical models as a function of the number of grid points per horizontal direction, the horizontal resolution of the atmospheric features, and the size of the domain which can be represented with such models. As discussed in Section 2b, at least four grid points are required to resolve an atmospheric feature adequately with a numerical model. Due to current computer limitations, a maximum number of 100 grid points per coordinate direction was assumed here for a three-dimensional simulation and 1000 grid points per coordinate direction for a two-dimensional simulation. Of course, with the development of more powerful computers, these upper limits should increase. These two constraints on the number of grid points result in the three horizontal lines in Figure 9. Note that both constraints are independent of the particular atmospheric phenomenon under consideration.

The left vertical line in Figure 9 arises from the restriction that the hydrostatic assumption should not be made for a horizontal grid size smaller than 2 km in the case of a shallow circulation such as a sea breeze. (For deeper atmospheric circulations, larger horizontal grid sizes would be required for the hydrostatic

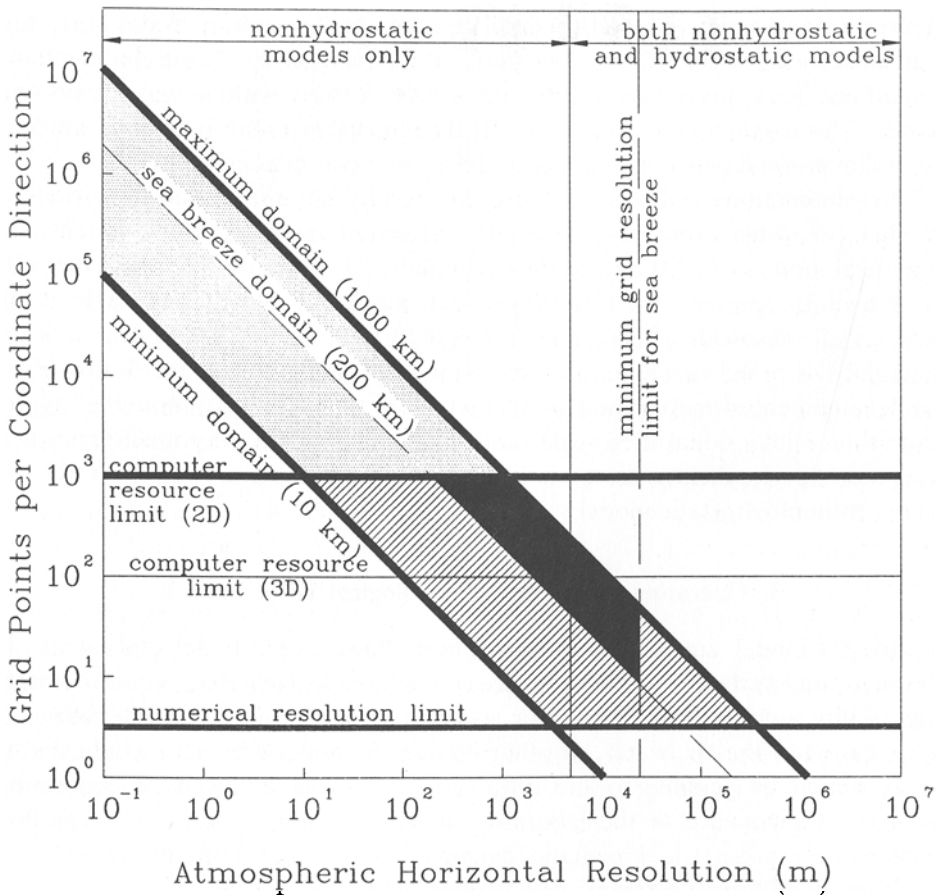


Fig. 9. The operating range (OR) of mesoscale numerical models for sea- and land-breeze simulations: number of model grid points per horizontal coordinate axis vs. atmospheric horizontal resolution. The stippled area denotes the potential OR for mesoscale numerical models in a homogeneous synoptic environment given more powerful computers. The hatched and blackened areas indicate the current mesoscale model OR. The blackened area denotes the current OR for SLB simulations.

assumption to hold). The right vertical line denotes a grid size of 20 km. Assuming a SLB horizontal extent of 80 km, this is the minimum or coarsest grid resolution (i.e., maximum grid spacing) which would give at least four horizontal grid points across the SLB circulation.

The three diagonal lines in Figure 9 represent the relationship between model resolution or grid size and the number of grid points required to represent the domain of interest. They correspond to a 10 km minimum horizontal domain size for control of domain-scale accelerations, a 200 km minimum horizontal domain size to encompass an entire mid-latitude SLB circulation system, and a 1000 km maximum horizontal domain size for use of a horizontally homogeneous background synoptic environment. For instance, with a model resolution of 10 m, the

number of grid points needed to simulate a sea breeze with a model horizontal domain size of 200 km is 20,000 per horizontal direction. Given present computer limitations, such resolution cannot be achieved even with a two-dimensional model. The maximum resolution for SLBs achievable today is about 2 km in a three-dimensional mesoscale model or 200 m in a two-dimensional model.

The combination of all of these constraints results in the solid black quadrilateral in Figure 9, which represents the OR of current two- and three-dimensional numerical models of SLB circulations. The hatched trapezoid (including the solid black region) represents the OR of mesoscale numerical models achievable at this time for all mesoscale phenomena, not just SLB's, and the stippled area is the potential OR of mesoscale models which might be achievable in the future, given the development of more powerful computers. It is interesting to note that hydrostatic three-dimensional mesoscale models will not benefit very much from new computer developments; most of the benefits from expanded model ORs will accrue to nonhydrostatic models.

3. Operating Range for Meteorological Wind Tunnels

In physical model simulations of atmospheric flows, scale-model replicas of observed ground-surface characteristics are constructed and inserted into a laboratory flow facility such as a wind tunnel or water channel. The flow characteristics and stratification of the air, water, or other fluid in the tank or tunnel are adjusted to be as similar as possible to the observed, large-scale atmospheric conditions. Complete equivalence of the laboratory *model* and atmospheric *prototype* flow fields requires geometric, kinematic, dynamic, and thermal similarity. In addition, boundary conditions upstream, downstream, at the lower surface, and near the top of the physical model must be similar to those at the corresponding boundaries of the modeled atmospheric domain. These multiple similarity requirements, the characteristics of the wind tunnel and its instrumentation, and the nature of the atmospheric phenomenon to be modeled all help to determine the OR for a wind-tunnel simulation.

a. GENERAL SIMILARITY REQUIREMENTS AND DIMENSIONLESS PARAMETERS

Geometric similitude exists between the laboratory model and its atmospheric prototype if the ratios of all corresponding spatial dimensions in model and prototype are equal. This is accomplished by using an undistorted scale model of the prototype geometry. Kinematic similitude exists between model and prototype if the paths of homologous particles, that is, particles with the same relative position, are geometrically similar and if the ratio of the velocities of homologous particles are equal. Dynamic similitude exists between geometrically and kinematically similar systems if the ratios of all homologous forces in model and prototype are the same. Thermal similitude requires buoyancy force to be in proper proportion to all other forces; thus, it is a component of dynamic similitude.

The similitude parameters governing the phenomenon of interest may be established by dimensional analysis. Based on dimensional analysis, dimensionless parameters such as Rossby number, Reynolds number, bulk Richardson number, Eckert number, Euler number, Prandtl number, Schmidt number, and Peclet number should each be the same for model and prototype if we want the two flow systems to be exactly similar.

Consider a steady, turbulent, near-neutral flow with representative velocity U_0 , length scale L_0 , rotation rate Ω_0 , kinematic viscosity (or momentum diffusivity) ν_0 , temperature T_0 , vertical temperature change ΔT_0 , downstream pressure change ΔP_0 , density ρ_0 , gravitational acceleration g , specific heat at constant pressure c_{p0} , molecular thermal diffusivity κ_0 , and molecular mass diffusivity α_0 . The dimensionless parameters will be defined by the following expressions:

| | |
|---------------------------------------|------------------------|
| $Ro = U_0/\Omega_0 L_0$ | Rossby number |
| $Re = U_0 L_0/\nu_0$ | Reynolds number |
| $Ri_B = g L_0 \Delta T_0 / T_0 U_0^2$ | bulk Richardson number |
| $Ec = U_0^2 / c_{p0} \Delta T_0$ | Eckert number |
| $Eu = \Delta P_0 / \rho_0 U_0^2$ | Euler number |
| $Pr = \nu_0 / \kappa_0$ | Prandtl number |
| $Sc = \nu_0 / \alpha_0$ | Schmidt number |
| $Pe = U_0 L_0 / \kappa_0$ | Peclet number. |

Equality of these similitude parameters for the two flow systems must be supplemented by the requirement that the surface boundary conditions and the approach-flow characteristics also be similar for the atmosphere and the physical model (e.g., Cermak, 1971; Snyder, 1972). Boundary-condition similarity requires similar values of

- Surface roughness,
- Topographic relief,
- Surface temperature distribution,
- Upstream distribution of mean and turbulent velocities,
- Upstream distribution of mean and turbulent temperatures, including inversion height, and
- Longitudinal pressure gradient.

If all of the above conditions are met simultaneously, then all scales of motion ranging from the atmospheric microscale to mesoscale (i.e., 10^{-3} m to 10^6 m) could be simulated exactly by the laboratory model. Unfortunately, not all of these similarity requirements can be satisfied simultaneously by a scaled model since some are incompatible or conflicting; only partial or approximate similarity can be achieved. This limitation strongly suggests that a laboratory model for a

particular meteorological or wind engineering situation be designed to simulate most accurately those scales of motion which are of greatest significance for the application. By considering each similarity requirement separately, it is possible to determine which flow features dominate and hence which similitude parameters are most important. Like the numerical modeler, the physical modeler must tailor his model to suit the problem of interest based on good judgment, theoretical understanding, physical intuition, and previous experience.

B. DYNAMIC SIMILARITY REQUIREMENTS ON INTERNAL TUNNEL FLOWS

The Rossby number (Ro) represents the ratio of local or advective accelerations to Coriolis accelerations. Rossby number equality is not possible in nonrotating laboratory facilities; hence, turning of the mean wind direction with height in the atmospheric boundary layer cannot be simulated. Accordingly, a wind-tunnel boundary layer is only an adequate model for atmospheric flow when either this effect is not significant for the application or when wind shear is small. In the case of SLB circulations, Coriolis effects are significant over longer times (e.g., 6–12 h), imposing a limit on the applicability of nonrotating laboratory analogs of these circulations.

The Reynolds number (Re) represents the ratio of inertial to viscous forces. Reynolds number equality is also not attainable due to the very high flow speeds which would be required in the laboratory flow as a result of the reduced length scale. However, this restriction does not seriously limit the simulation of SLB circulations since the significant mean flow characteristics are only weakly dependent upon the Reynolds number. For instance, the total surface drag coefficient for a given ratio of boundary length to roughness length, L/z_0 , becomes invariant with respect to the wind-tunnel Reynolds number well within the typical meteorological wind-tunnel Reynolds number range (Cermak, 1975). This concept of Reynolds number independence was first advanced by Townsend (1956) and implies that the gross structure of turbulence is similar over a wide range of Reynolds numbers. Two exceptions are flow features related to very small-scale turbulence and the laminar sublayer adjacent to boundaries (Snyder, 1972; Meroney, 1986). The latter exception is avoided if boundaries are aerodynamically rough (see next section).

The bulk Richardson number (Ri_B) compares the importance of buoyancy to inertial forces and is an important parameter in stratified-flow modeling. It is equal to the inverse square of the densimetric Froude number, $Fr = U_0/(gL_0\Delta T_0/T_0)^{1/2}$. Specially constructed wind tunnels can produce bulk Richardson numbers ranging from -0.5 to 0.5 . These Ri_B values cover a wide range of atmospheric conditions. Meroney (1986) pointed out that equality of Richardson number imposes low fluid-model wind speeds in order to use reasonable vertical temperature differences, thus reducing the model Reynolds number. Such conflicting relationships make it impossible to obtain simultaneous similitude in all relevant similarity parameters. Batchelor (1953) discussed the conditions under which Richardson

number is the sole global governing criterion for dynamical similarity of motion in a perfect-gas atmosphere.

The Eckert number (Ec) indicates the ratio of kinetic to excess internal energy. Equal Eckert numbers are not possible when equal Richardson numbers are achieved. Instead, the model Eckert number will be about one order of magnitude smaller than the atmospheric value (Cermak, 1982). However, the Eckert number is equivalent to a Mach number squared. Thus, it is small compared to unity for both atmospheric and laboratory flows.

The Euler number (Eu) compares the relative magnitude of pressure-fluctuation-induced accelerations and inertial accelerations. This parameter is of order one and is automatically simulated in air. However, wind-tunnel blockage due to insertion of model buildings or three-dimensional topography in the tunnel may induce longitudinal pressure gradients unless the tunnel sidewalls or ceiling can be adjusted to compensate (e.g., Cermak, 1971).

The Prandtl number (Pr) is the ratio of momentum diffusivity to thermal diffusivity. It indicates the relative ability of a fluid to transport momentum and heat via molecular processes. For air, the Prandtl number does not vary strongly with temperature. Thus, Prandtl numbers are essentially equal for flows in the atmosphere and the typical meteorological wind tunnel.

Like the Prandtl number, the Schmidt number (Sc) is a fluid property rather than a flow property. It is the ratio of momentum diffusivity to mass diffusivity or, alternatively, the ratio of molecular momentum transport to molecular mass transport. It is an important parameter for studies of the transport of a passive scalar quantity. The Schmidt number is close to unity for most gases.

The Peclet number (Pe) is a measure of the ability of the fluid to transport heat or mass by advection compared to molecular diffusion. It may also be expressed as the product of a Reynolds number and either a Prandtl number ($RePr$) or Schmidt number ($ReSc$), depending upon whether heat or mass transport is being considered. At high Reynolds numbers, turbulent diffusion will overwhelm molecular diffusion. Thus, in general, the Peclet number for heat and mass transport is not important if the flow exhibits Reynolds number independence (Snyder, 1972).

C. BOUNDARY-CONDITION SIMILARITY REQUIREMENTS

When the prototype and model flows are thermally stratified, there are additional similarity requirements which should be considered. Yamada and Meroney (1971), SethuRaman and Cermak (1974, 1975), and Ogawa *et al.* (1975) have discussed problems in achieving similarity of stratified flow motion over regions of nonhomogeneous heating such as coasts. They pointed out that approximate dynamic similarity can be achieved by requiring equality of the upstream bulk Richardson number,

$$Ri_B = \frac{g \Delta T H}{\bar{T} U^2}, \quad (6)$$

or, equivalently, the densimetric Froude number, for the wind-tunnel flow and the coastal circulation. In this expression, H is a vertical length scale (often the height of an inversion), ΔT is the difference at the upstream entrance between mean temperature (potential temperature in the case of the atmosphere) at the surface and at height H , \bar{T} is the average temperature over the layer of depth H , U is the velocity at height H , and g is the gravitational acceleration. Thus, Equation (6) is an upstream-boundary-condition similarity requirement.

Another similarity factor which could be considered in SLB simulations is the heat transfer rate from sea and land surfaces to the atmosphere. This quantity may be characterized by the ratio of a characteristic vertical length scale H to the Monin-Obukhov length scale,

$$H/L_{MO} = H/[-u_*^3 \bar{\rho} c_p \bar{T}/(kgq)], \quad (7)$$

where u_* is the friction velocity, $\bar{\rho}$ is the average air density, c_p is the average specific heat at constant pressure, \bar{T} is the average near-surface temperature, k is the von Kármán constant, g is the gravitational acceleration, and q is the surface heat flux (Meroney *et al.*, 1975a). This parameter would be of particular importance in coastal fumigation simulations. Note, however, that the Monin-Obukhov length scale L_{MO} may vary locally as one moves inland from the shoreline.

The similarity between the flow-generating mechanisms of sea breezes and flow over urban heat islands suggests an alternative parameter. Linear numerical analysis by Olfe and Lee (1971) and experimental and numerical studies by Yamada and Meroney (1971) suggest that the intensity of heating by the land surface may be characterized by a heating ratio,

$$R_H = \frac{(T_{\text{land}} - T_{\text{sea}})_{\text{surface}} H}{(T_{z=H} - T_{z=z_0})_{\text{sea}} L}. \quad (8)$$

Since the vertical-to-horizontal modeling scale ratio H/L is normally undistorted, this parameter reduces to a single temperature ratio. Meroney *et al.* (1975a) suggested that typical coastal values are $R_H = 1.3-1.9$ and $Ri_B = 1.25-1.5$, where $H = 400$ m. Laboratory conditions should be chosen to simulate these situations as closely as possible. Note that Equation (7) is a lower-boundary-condition similarity requirement while Equation (8) is a combined upstream-boundary-condition/lower-boundary-condition similarity requirement.

There is a minimum Reynolds number below which the gross flow characteristics of the boundary layer are not invariant. Most investigators, beginning with Sutton (1949), have required that the turbulence Reynolds number or surface Reynolds number $Re_* = u_* z_0/\nu$ be larger than 2.5 for Reynolds number independence to hold, where u_* is the friction velocity, z_0 is the roughness length, and ν is the kinematic viscosity. The value 2.5 is an empirically determined constant. For $Re_* < 2.5$, it has been observed that mean velocity profiles in turbulent pipe flow lose similarity in shape and deviate from the universal curve for a rough-wall turbulent

boundary layer (e.g., Sutton, 1949; Snyder, 1972). When $Re_* > 2.5$, the surface is said to be aerodynamically rough. Since virtually all natural geophysical surfaces are aerodynamically rough, the flow structures related to momentum transfer will be similar if the scaled roughness yields a sufficiently small value for the ratio of boundary length to roughness length, L/z_0 . Should the resulting model L/z_0 be too large, then the model roughness can be exaggerated to produce an aerodynamically rough surface.

Although turbulent mixing may be scaled properly in a wind tunnel for Reynolds-number-independent flow, problems may still arise due to the proportionately larger contribution of molecular diffusion. Experiments by Crapper and Linden (1974) suggested that the structure of a density turbulence interface is altered by molecular diffusion for Peclet numbers less than 200. However, a better parameter to assess the influence of molecular diffusivity on the rate of mixing may be the ratio of Peclet number to Richardson number. Puttock and Colenbrander (1985) suggested a critical value of 1500 for this ratio $Pe/Ri = U^3/g'\alpha$, where U is the mean model velocity at a height of 10 cm, g' is the buoyancy-modified acceleration due to gravity, and α is the molecular diffusivity. Meroney (1987) proposed a corresponding critical value of 0.2 for the surface ratio Pe_*/Ri_* , where molecular diffusion becomes significant for Pe_*/Ri_* values less than 0.2.

D. INSTRUMENTATION CHARACTERISTICS

Hot-wire, hot-film, and pulsed-wire anemometers are available to measure wind speed and turbulence in wind tunnels (e.g., Hinze, 1975). Pitot tubes are rarely usable at the low speeds required for wind-tunnel simulation of SLB circulations. Laser anemometry may be used at low flow velocities, but adequate traverse systems with good positioning capabilities are rarely installed in the larger meteorological facilities. Thermocouples and thermistors are used to measure temperature profiles in meteorological wind tunnels capable of thermal stratification. The following experimental limitations should be considered when one proposes laboratory measurements: measurement accuracy; averaging times and sampling rates; and spatial resolution.

1. *Measurement Accuracy*

Measurement accuracy is an important factor for wind-tunnel modeling of SLBs. The flow speeds required for the simulation of such circulation systems are often less than 0.5 m s^{-1} . Most conventional hot-wire or hot-film instruments are not reliable at such low velocities. Care must be taken to achieve reliable calibration, to correct for low-speed probe nonlinearity, and to avoid electronic noise in this low-signal regime. The pulsed-wire anemometer is especially useful for low-speed and reversing flows since it can detect the direction of flow (Bradbury and Castro, 1971).

2. Averaging Times and Sampling Rates

There are two questions which arise with respect to averaging times associated with laboratory measurements. First, to what prototype averaging time is the laboratory measurement equivalent, and second, how long should one sample in the laboratory to obtain a stable average? Let us consider an atmospheric measurement made at a height of 10 m for a wind speed of 3 m s^{-1} . Assuming a typical eddy scale of 10 m, one finds that a 15-min average allows one to sample 270 eddies carried past the fixed instrument by the mean wind. Given a model scale of 1:200 so that the equivalent boundary-layer position is 5 cm, then a 30-sec average in the laboratory will sample a comparable number of eddies (300) for a model wind speed of 0.5 m s^{-1} .

Lumley and Panofsky (1964) showed how averaging time requirements can be related to turbulence scales. Given a steady turbulent shear flow, the turbulence can be presumed drawn from a Gaussian probability distribution. Near a wall in a turbulent boundary layer, a typical averaging time T_U can be obtained from the following equation:

$$T_U = 2i^2(\delta/U)/\epsilon^2, \quad (9)$$

where δ is the tunnel boundary-layer depth, U is the mean flow speed, i is the turbulence intensity $(\overline{u'^2})^{1/2}/U$, and ϵ is the fractional error (i.e., normalized by \bar{U}) of the difference between the velocity ensemble average, \bar{U} , and the estimate obtained by integration over the averaging time T_U . Hence, for $\delta = 1 \text{ m}$, $U = 0.5 \text{ m s}^{-1}$, and $i = 0.1$, then $T_U = 0.04/\epsilon^2$. When ϵ is equal to 1, 5, and 10%, T_U will equal 400, 16, and 4 s, respectively (Meroney, 1987).

3. Spatial Resolution

Hinze (1975, p. 120) has considered the influence of hot-wire length on the contribution of high-frequency fluctuations to estimates of turbulent energy, $\overline{e'^2}$. He pointed out that in order to correct the transducer for spatial resolution, the measured values must be adjusted by a correction factor CF. When the transducer size \cap is much greater than the turbulence integral length scale Λ_g , the correction is very large and no turbulence is measured. When \cap is less than λ_g , the Taylor microscale, the eddy spatial correlation $g(x) = (1 - x^2/\lambda_g^2)$ and we have

$$\text{CF} = \left(1 - \frac{\cap^2}{6\lambda_g^2}\right)^{-1}. \quad (10)$$

Note that the correction is on $\overline{e'^2}$, not e' ; that is, the smallest eddies may be smaller than the Taylor microscale or dissipation scale λ_g . Nonetheless, one sees that if $\cap < 0.5\lambda_g$, only a 4% spatial resolution error exists in $\overline{e'^2}$, and if $\cap \approx \lambda_g$, a 20% error in $\overline{e'^2}$ would occur. Meroney (1987) has discussed Hinze's CF factor in the context of measurements of concentration variance $\overline{c'^2}$.

Li and Meroney (1985) measured Taylor microscales between 0.015 and 0.033 m

in a meteorological wind tunnel at wind speeds below 2 m s^{-1} . Neff and Meroney (1982) estimated sampling areas of their aspirated hot-film katherometers to be less than 0.5 cm^2 . Given $\lambda_g = 0.02 \text{ m}$ and $\cap = 0.007 \text{ m}$, the instrument would measure velocity variance with only a $\pm 2\%$ error due to spatial resolution.

E. WIND-TUNNEL CHARACTERISTICS

The viability of a given simulation scenario is not only a function of the governing flow physics but also depends on the availability of a suitable simulation facility and the characteristics of the measurement instrumentation to be employed. It would seem appropriate, therefore, to suggest bounds for the range of atmospheric situations which can be reasonably treated by wind-tunnel modeling. Boundary-layer wind tunnels exist at various laboratories. Generally, these tunnels range in size from facilities with working cross sections of $0.5 \times 0.5 \text{ m}$ to those with working cross sections of $3 \times 4 \text{ m}$ (Meroney, 1987). Several of these facilities are equipped with movable side walls or ceilings to adjust for model blockage and ensure Euler number similarity. By using vortex generators, fences, roughness elements, grids, screens or jets, a wide range of turbulence integral scales can be introduced into the tunnel boundary layer (e.g., Armitt and Counihan, 1968, Méry *et al.*, 1974; Meroney, 1987). Choice of model surface roughness permits control of surface turbulence intensity, dimensionless wall shear, and velocity profile shape. Density stratification can be induced by use of heat exchangers, injection of heated air, gases of different molecular weight, or latent heat absorption or release during phase change (e.g., Ogawa *et al.*, 1985; Meroney, 1986).

The characteristics of an individual wind tunnel will determine its overall operating range or performance envelope. For instance, the meteorological wind tunnel (MWT) at Colorado State University is a large, closed-circuit facility with a 1.8 m high by 1.8 m wide by 24 m long test section. Wind speeds are continuously variable from 0.1 to 30 m s^{-1} and ambient air temperatures can be varied from 5 to $205 \text{ }^\circ\text{C}$ (e.g., Cermak, 1975, 1982). The ceiling is adjustable to permit reduction of the longitudinal pressure gradient to zero. Ten meters of the upstream test-section floor can be cooled between $1 \text{ }^\circ\text{C}$ and ambient temperature while 12 m of the downstream test-section floor can be heated from 1 to $200 \text{ }^\circ\text{C}$.

The following criteria have been selected to specify the MWT operational range:

- Maximum model obstacle height $h_m < 0.5 \text{ m}$,
- Minimum model obstacle height $h_m > 0.02 \text{ m}$,
- Maximum model blockage $< 10\%$,
- Minimum model Reynolds number $(\text{Re}_h)_m = U_m h_m / \nu_m > 10,000$,
- Maximum model turbulence integral scale $(\Lambda_U)_m < 0.5 \text{ m}$,
- Minimum model turbulence integral scale $(\Lambda_U)_m > 0.05 \text{ m}$,
- Minimum model measurement resolution $(\Delta z)_m > 0.0001 \text{ m}$,
- Maximum model boundary-layer depth $\delta_m < 2 \text{ m}$, and
- Minimum model boundary-layer depth $\delta_m > 0.1 \text{ m}$.

Based on Coriolis force considerations, Snyder (1972) suggests a 5 km maximum cut-off point for horizontal length scales for modeling atmospheric diffusion, Méry *et al.* (1974) suggest a 15 km limit, Ukeguchi *et al.* (1967) suggest a 40 to 50 km limit, and Cermak *et al.* (1966) recommend a 150 km limit. A middle estimate would be that of Orgill (1971), who suggests that a horizontal length scale of up to 50 km is not unreasonable for complex terrain in strong winds.

F. WIND-TUNNEL OPERATING RANGE FOR SLB SIMULATIONS

The most fundamental restrictions on the wind-tunnel operating range or performance envelope result from geometric similarity constraints. Suppose the atmospheric boundary-layer depth δ_p falls in the 200 to 1,000 m range and the atmospheric longitudinal integral velocity scale $(L_U)_p$ falls in the 100 to 1,000 m range. Given the wind-tunnel size constraints from Section 3e, then δ_p/δ_m must lie between 100 and 10,000 and $(L_U)_p/(L_U)_m$ must lie between 200 and 20,000, restricting the simulation length-scale ratio (LSR) to the 200 to 10,000 range. Since the CSU meteorological-wind-tunnel test section is 1.8 m by 1.8 m by 25 m, the corresponding atmospheric domain size will lie in the 0.36–18 km by 0.36–18 km by 5–250 km range. If we restrict our atmospheric domain size to 50 km because of the Rossby number restriction, we reduce the LSR upper limit to 2,000.

Based on the previous discussion, the following five dynamic similarity criteria appear pertinent to the physical simulation of SLB circulations:

1. $(\text{Ri}_B)_m = (\text{Ri}_B)_p$;
2. $(\text{Re}_*)_m > A$, where $1 < A < 5$ and $\text{Re}_* = u_* z_0 / \nu$;
3. $(\text{Pe}_*/\text{Ri}_*)_m > B$, where $0.14 < B < 0.2$, $\text{Pe}_*/\text{Ri}_* = u_*^3/g'\alpha$, and $g' = (\Delta T/\bar{T})g$;
4. $(L/L_{\text{MO}})_m = (L/L_{\text{MO}})_p$ or $(R_H)_m = (R_H)_p$; and
5. Similar upwind velocity, temperature, and turbulence profiles.

In a coastal flow, mechanical and thermal turbulence influence one another. Surface temperature variations between the land and the sea alter turbulence structure, and turbulence in turn alters the velocity and temperature profiles. Thus, the temperature and velocity fields are not independent. Using Equation (6), bulk Richardson number equality (Criterion 1) requires that

$$\text{LSR} = \frac{H_p}{H_m} = \left(\frac{\Delta T}{\bar{T}} \right)_m \left(\frac{\bar{T}}{\Delta T} \right)_p \left(\frac{U_p}{U_m} \right)^2, \quad (11)$$

where LSR denotes the prototype-to-model vertical length-scale ratio.

The requirement that the surface or roughness Reynolds number Re_* be large enough to ensure fully rough flow (Criterion 2) is also satisfied if one stipulates model conditions such that

$$\text{LSR} < \left(\frac{C_{fm}}{2} \frac{\Delta T_m}{\Delta T_p} \frac{\bar{T}_p}{\bar{T}_m} \right)^{1/3} \left(\frac{U_p z_{0p}}{\nu_m A} \right)^{2/3}, \quad (12)$$

where the model skin friction coefficient $C_{fm} = 2u_{*m}^2/U_m^2$ and Equation (11) has been used to convert U_m to U_p .

The parameter Pe/Ri measures the relative rates of turbulent entrainment and molecular diffusion. If this parameter is too small, the scaled turbulent diffusion will be artificially enhanced by molecular diffusion and hence scaled concentrations will be too small and the inland growth of the coastal internal boundary layer may not be modeled correctly. To avoid this problem, the surface Peclet/Richardson number ratio Pe_*/Ri_* must also be sufficiently large (Criterion 3). Combining Criterion 3 and Criterion 1 yields the constraint

$$LSR < \frac{C_{fm}}{2(g\alpha_m B)^{2/3}} \left(\frac{\Delta T_m}{\bar{T}_m} \right)^{1/3} \left(\frac{\bar{T}_p}{\Delta T_p} \right) U_p^2. \quad (13)$$

From the Monin–Obukhov length-scale ratio (Criterion 4), another constraint on the wind-tunnel length-scale ratio LSR can be identified using Equation (7), namely that

$$LSR \leq \frac{(\bar{\rho}c_p\bar{T})_p}{(\bar{\rho}c_p\bar{T})_m} \left(\frac{q_m}{q_p} \right) \left(\frac{U_p}{U_m} \right)^3. \quad (14)$$

From sea-breeze observations, we know that prototype wind velocities range from 0.5 m s^{-1} to 12 m s^{-1} , prototype temperatures range from 5°C to 35°C , and prototype temperature differences between land and sea range from 1°C to 15°C (e.g., Atkinson, 1981). Meteorological wind tunnels can operate over a wider range for all three of these quantities (see Section 3e). However, practical limitations due to the characteristics of stratified-flow wind tunnels and their instrumentation restrict this range. In order to ensure measurement reliability and flow stationarity and to avoid too-high operating costs, current constraints for the MWT include $U_m \geq 0.5 \text{ m s}^{-1}$, $\bar{T}_m \leq 100^\circ\text{C}$, and $q_m \leq 50 \text{ W m}^{-2}$. Combining the similarity constraints given by Equations (11) and (12) with these wind-tunnel limits and typical atmospheric SLB conditions provides the relationships and data needed to construct the wind-tunnel OR and to identify reasonable simulation scenarios. Figure 10 suggests that wind-tunnel simulations of sea breezes can be attained over the following prototype data range: $2 \text{ m s}^{-1} < U_p < 15 \text{ m s}^{-1}$, $5^\circ\text{C} < T_p < 35^\circ\text{C}$ and $\Delta T_p < 15^\circ\text{C}$, given length-scale ratios between 200 and 1,000. The two curves in Figure 10 based on Equation (11) partition achievable and unachievable length-scale ratio and prototype flow velocity combinations for $\bar{T}_m = \bar{T}_p$ given $(\Delta T)_p$, a maximum $(\Delta T)_m$ of 80°C , and a minimum U_m of 0.5 m s^{-1} . The two curves for Equation (12) were calculated assuming $C_{fm} = 0.005$, $\nu = 1.5 \times 10^{-5} \text{ m}^2 \text{ s}^{-1}$, and $(z_0)_p = 0.1 \text{ m}$.

Laboratory instrument size constrains the finest spatial resolution achievable for predictions of prototype flow variables. For example, we know that the maximum¹

¹ Experimentalists will probably prefer the use of the term ‘minimum resolution’ here but we are using ‘maximum resolution’ in the numerical modeler’s sense of finest, highest, greatest, or best resolution.

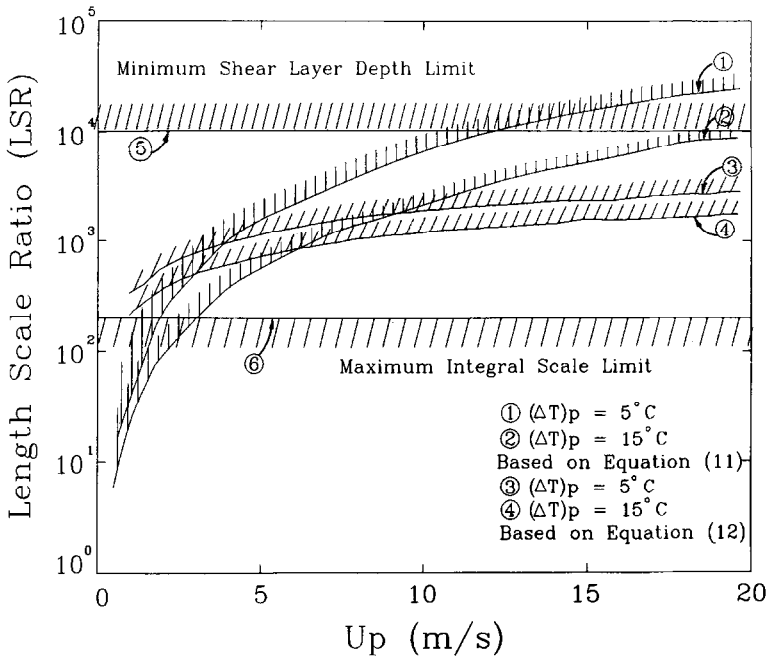


Fig. 10. Operating-range constraints for wind-tunnel modeling of sea breezes: length-scale ratio (LSR) vs. prototype wind speed (U_p). Curves (1) and (2) result from Equation (11) using $(\Delta T)_p$ values of 5°C and 15°C , respectively, and assuming $\bar{T}_m = \bar{T}_p$, $(\Delta T)_m = 80^\circ\text{C}$, and $U_m = 0.5\text{ m s}^{-1}$. Curves (3) and (4) result from Equation (12) and the same parameter values used to obtain curves (1) and (2), respectively. Line (5) arises from the minimum geometric similarity constraint on PBL depth (LSR = 10,000). Line (6) arises from the maximum geometric similarity constraint on integral length scale (LSR = 200).

linear resolution (i.e., smallest separation between measurement points) for the X -wire measurement of velocity and turbulence in the MWT ranges from 1 to 2 mm. Given a LSR range of 200 to 2,000, this corresponds to a maximum atmospheric linear resolution range of 0.4 to 4 m. If we require four adjacent measurements to resolve a mean model flow feature and make allowances for instrument positioning error, this gives a minimum wind-tunnel domain size of 1 cm. For a LSR value of 200, this corresponds to a minimum atmospheric domain size of 2 m. For a LSR value of 2,000, the corresponding minimum atmospheric domain size would be 20 m.

The number of measurements that can be made in a physical model is limited by the finite time taken to record each point. As noted in Section 3d, reliable model time averages require an average measurement time of 30 s. Thus, acquisition of 1,000 sample points with X -wire anemometry would require an 8-hour wind-tunnel sampling period. This number of sample points has been taken as a practical maximum limit. For longer sampling periods, questions of wind-tunnel stationarity, reliability, operating expense, and availability begin to become important.

If we combine all of these constraints, we obtain Figure 11, a counterpart to Figure 9. The vertical axis in Figure 11 is proportional to the number of measurement points. As in Figure 9, one horizontal axis in Figure 11 corresponds to atmospheric or prototype horizontal resolution. However, an additional axis is required in Figure 11 to show length-scale ratio. This third axis is not needed in Figure 9 because numerical models are implicitly full-scale models with LSR equal to unity. Thus, the OR shown schematically in Figure 11 is a volume rather than an area as in Figure 9.

The two horizontal lines in Figure 11 for a given LSR value are analogous to the horizontal lines in Figure 9. The lower horizontal line marks the measurement resolution limit, that is, the minimum number of adjacent measurement points (4) needed to resolve a flow feature. The upper line denotes the practical present-day upper bound on the number of measurement points sampled in one wind-tunnel run. The vertical lines in Figure 11 represent the maximum prototype resolution (i.e., finest detail) which can be modeled for a given LSR due to instrument limitations. The lower diagonal lines mark the smallest atmospheric domain size which can be represented in the wind tunnel for a given LSR value, a given number of measurement points, and a linear sampling strategy; this bound is also

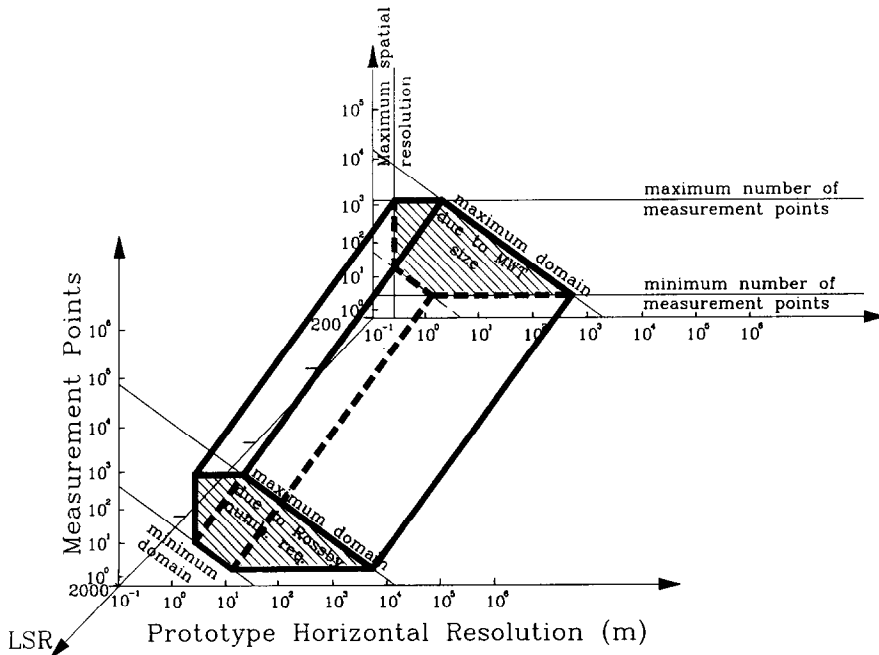


Fig. 11. Operating range for wind-tunnel modeling of sea breezes: number of measurement points vs. prototype horizontal resolution vs. length-scale ratio. The hatched polygon in the foreground corresponds to a LSR of 2,000, the one in the background to a LSR of 200.

due to instrument limitations. As in Figure 9, the upper diagonal lines represent maximum prototype domain limits, in this case the 50 km limit due to Rossby number considerations. Thus, for the applicable geometric and dynamic similarity constraints, longitudinal atmospheric domain sizes between 2 m and 50 km appear to be the model simulation limits for a meteorological wind tunnel with a 25 m test section. The size of the smallest resolvable atmospheric feature (and hence the smallest domain size) ranges between 2 m and 20 m depending on the LSR selected.

Note that the wind-tunnel simulations assume steady approach flow and surface conditions. However, one can synthesize the average statistics of a wind-tunnel flow field over longer time periods by associating a given measurement set with a recurring meteorological situation for which climatological probability distribution information is available. (A similar approach has been taken in applying mesoscale meteorological models to longer time periods, e.g., Pielke, 1982). In addition, wind-tunnel results simulate the average of many realizations of the air flow over a coastal region whose boundary and initial conditions are 'near' those of the laboratory model. Any single realization of the air flow over a coastal region thus has a finite probability of varying from the mean behavior.

4. The Relationship Between Numerical and Physical Models of Sea and Land Breezes

A complete model to simulate a sea breeze or land breeze should be able to:

1. Simulate the full SLB circulation system;
2. Simulate the small-scale shear flow motions and turbulent transport; and
3. Simulate the interaction between these two scales of motion.

In the absence of significant larger-scale flow, the sea-breeze circulation consists of a landward current near the surface and an upper-level seaward return flow which is about twice the depth and half the speed of the landward current. The SLB circulation may reach 200 km in horizontal extent and 2 or 3 km in vertical extent. In a conventional meteorological wind tunnel, it is not possible to simulate the upper-level return flow nor the phenomena of wind veering with height, radiational cooling, or phase changes. In contrast, Pielke (1984) notes that numerical mesoscale models have successfully simulated the mesoscale characteristics and structure of SLB circulations. Thus, the numerical model provides a way to generate realistic velocity, temperature, and constituent profiles for use as boundary conditions in a physical model.

However, in a coastal region, there is usually a large spatial variance in surface roughness and heat capacity. The interaction of the production and dissipation of turbulence in this region is very complex. In the case of a sea breeze, when marine air flows over warmer land, mechanical shear and buoyancy forces both act to increase turbulence energy. However, when air flows over the colder sea surface

in a land breeze, mechanical turbulence interacts with the stably stratified flow to dissipate the turbulence energy. Thus, the interaction between turbulence and stratification is an important factor in the growth of a thermal internal boundary layer near the coast. Three questions naturally arise concerning the sea-land transition zone:

1. Is there a consistent tendency for variations in the boundary layer to be associated with surface variations?
2. Do the surface variations change the turbulence profiles?
3. If so, how do the inhomogeneous surface heat flux and roughness changes influence profiles of various turbulence statistics?

These questions are difficult to address with a numerical model because of the very high spatial resolution required. For instance, Durand *et al.* (1989) have recently described the numerical simulation of a TIBL associated with onshore flow across the Dutch coast. They used a two-dimensional, hydrostatic mesoscale model with a third-order turbulence closure scheme, 2 km horizontal grid spacing, and 50 m vertical grid spacing. General features of the TIBL turbulence field were reproduced despite the quite coarse horizontal resolution. However, improving the horizontal resolution would likely require switching to a nonhydrostatic model and to a larger computer.

Hadfield (1988) used a large-eddy simulation model with $125 \times 125 \times 60$ m spatial resolution and a $4.5 \times 4.5 \times 2.3$ km domain to study convective boundary layer (CBL) development and structure over inhomogeneous terrain. This numerical model required use of a Cray X-MP/48 computer and will be taken as representative of the present generation of highest-resolution PBL models. Hadfield obtained many interesting results and good agreement with CBL observations but there were still some differences: potential temperature variance and pressure variance were too small, vertical velocity skewness was too large in the upper half of the simulated boundary layer, and the horizontal velocity variance profile had too pronounced a maximum near the surface. Inadequate spatial resolution may have been an important source of these differences. Cyclic lateral boundary conditions were also employed, an unacceptable choice for SLB simulations. Thus, current numerical models have some difficulties in addressing question 2. New computers may make it possible to increase the spatial resolution of numerical models by a factor of two or more, but achieving 50 m horizontal resolution will require heroic efforts. In contrast, wind tunnels appear capable of 2 m horizontal resolution. Thus, the wind tunnel is a powerful tool with which to study the small-scale characteristics of air flow over coastal regions.

Spatial sampling strategy should also be considered. In Figure 11, 1,000 measurement points were taken as a practical upper bound for wind-tunnel simulations versus 100 grid points per axis for three-dimensional numerical simulations. If sampling is performed along a single measurement axis over only a portion of the domain, then the wind-tunnel spatial resolution will be orders of magnitude better

(i.e., finer) than that of the numerical model. If sampling is done at evenly-spaced points throughout the test-section volume, however, then the wind-tunnel spatial resolution will be worse than that of the numerical model. Vertical profiles and fluxes are normally of greatest interest so that a linear sampling strategy over a test-section subdomain will usually be the preferred wind-tunnel sampling strategy.

One restriction imposed on wind-tunnel simulations by the Reynolds number criterion is the need to run with at least a minimum flow speed in order to maintain turbulent flow. As shown in Figure 10, this implies some background flow speed in the atmospheric prototype so that sea-breeze cases in a stagnant environment cannot be modelled in the wind tunnel. Mitsumoto *et al.* (1983) avoided this restriction in their water tank simulations but at the cost of losing Reynolds number similarity. If physical models are to be used to help develop and/or verify turbulence parameterizations in mesoscale numerical models, the Reynolds number is a crucial similitude parameter.

One advantage of meteorological wind tunnels is that they do produce real

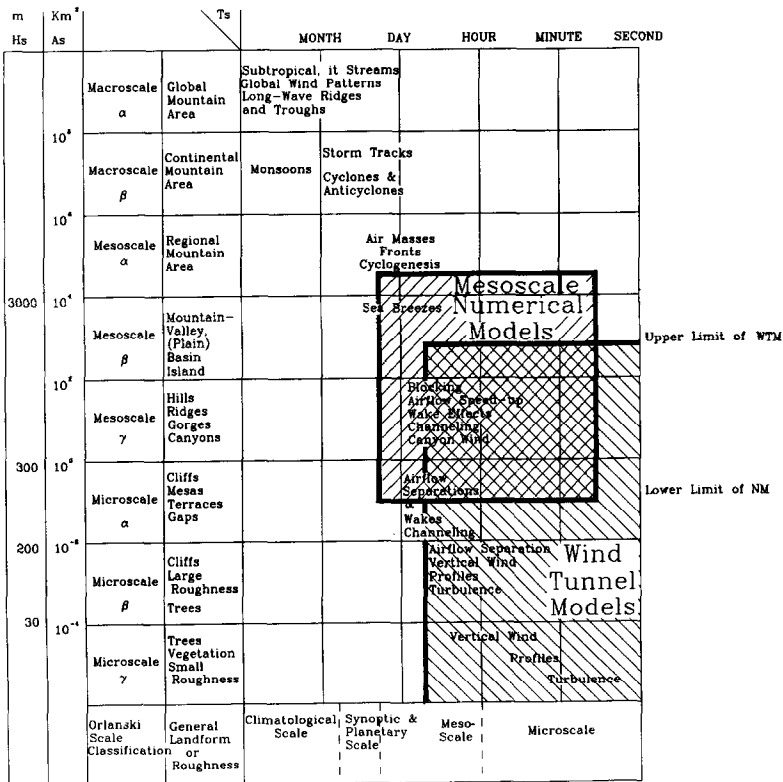


Fig. 12. Operating ranges for numerical and wind-tunnel modeling relative to the time and space continuum of atmospheric circulation systems. The crosshatched area shows the region of overlap for the two approaches. H_s denotes the representative depth scale, A_s the representative area scale, and T_s the representative time scale (after Orlanski, 1975 and Meroney, 1981).

turbulent flows. Almost all mesoscale numerical models employ ensemble-average turbulence parameterization schemes in which all randomness has been removed by implicitly averaging flow fields over an infinite ensemble of realizations (Wyn-gaard, 1982). Flow fields in most mesoscale numerical models will thus remain steady if all boundary conditions are held constant while wind-tunnel flows will exhibit time-dependent fluctuations for comparable conditions. This means that flow turbulence and its effects can be studied directly with a wind tunnel but only indirectly simulated with an ensemble-average mesoscale numerical model.

Meroney *et al.* (1978) and Meroney (1981) suggested qualitative operating ranges for meteorological wind tunnels in terms of the characteristic time and horizontal scales defined by Orlanski (1975) for the atmospheric flow continuum. Figure 12

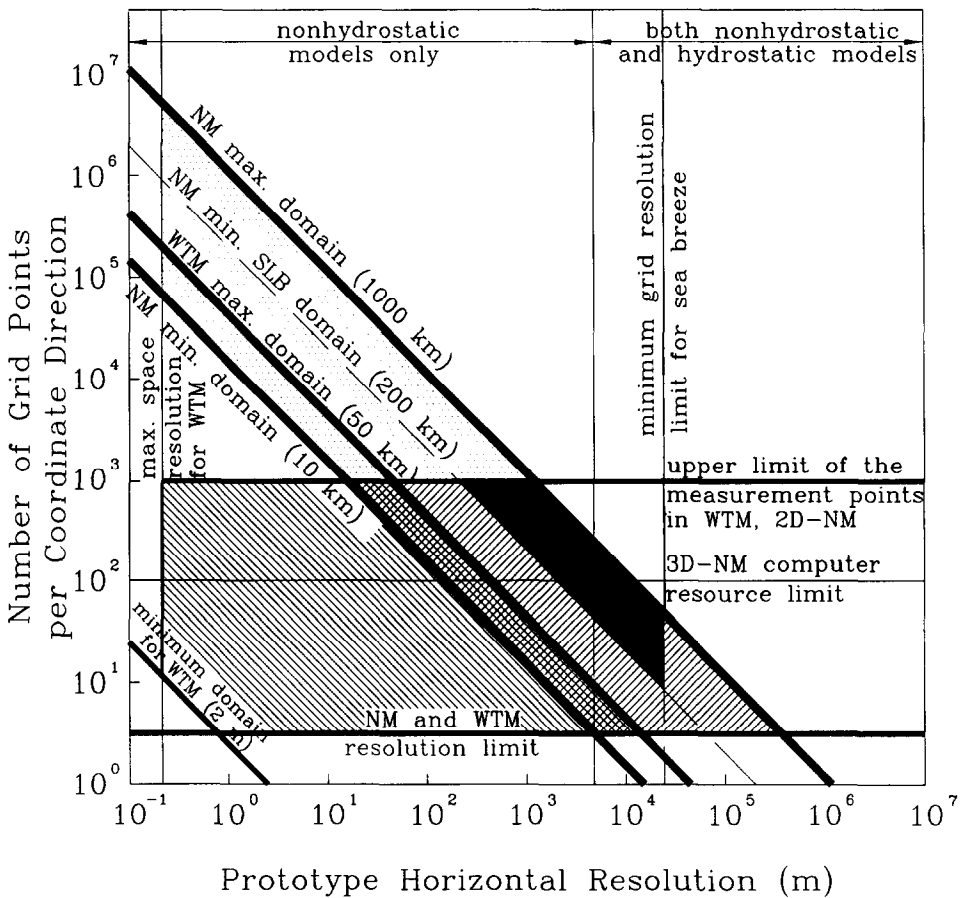


Fig. 13. Operating ranges for numerical and wind-tunnel modeling of sea breezes: number of grid/measurement points vs. atmospheric horizontal resolution. 'WTM' denotes 'wind-tunnel model'; 'NM' denotes 'numerical model'. The crosshatched area marks the common OR for numerical and wind-tunnel SLB simulations. Note that the OR volume shown in Figure 11 has been projected parallel to the LSR axis in order to obtain an OR 'area' comparable to that of Figure 9.

shows an updated version of this figure to which a qualitative mesoscale numerical model OR has been added. This figure suggests that mesoscale numerical models and meteorological wind tunnels should have an overlapping or common OR in addition to OR regions in which only one of the two modeling approaches would be suitable.

Figure 13 shows the corresponding combined performance envelopes for both modeling techniques based on the analysis of Sections 2 and 3 and Figures 9 and 11. It is thus more quantitative than Figure 12. From Figure 13, we can see that there is again an OR common to both models as well as OR regions exclusive to one approach. Wind tunnels cannot simulate a full SLB circulation and still maintain Rossby number similarity, but they can resolve smaller spatial scales than present numerical models. Numerical models can simulate complete SLB circulations but have difficulty in resolving smaller-scale SLB features such as the coastal internal boundary layer, an important flow feature for pollutant dispersion or wind energy generation near coasts.

Another important aspect of sea-breeze behavior is its time-dependent nature. Development of a controlled but unsteady wind-tunnel flow is a challenge for the future. It is not currently possible to use a wind tunnel to simulate the time evolution of the sea breeze. But numerical models can provide information about

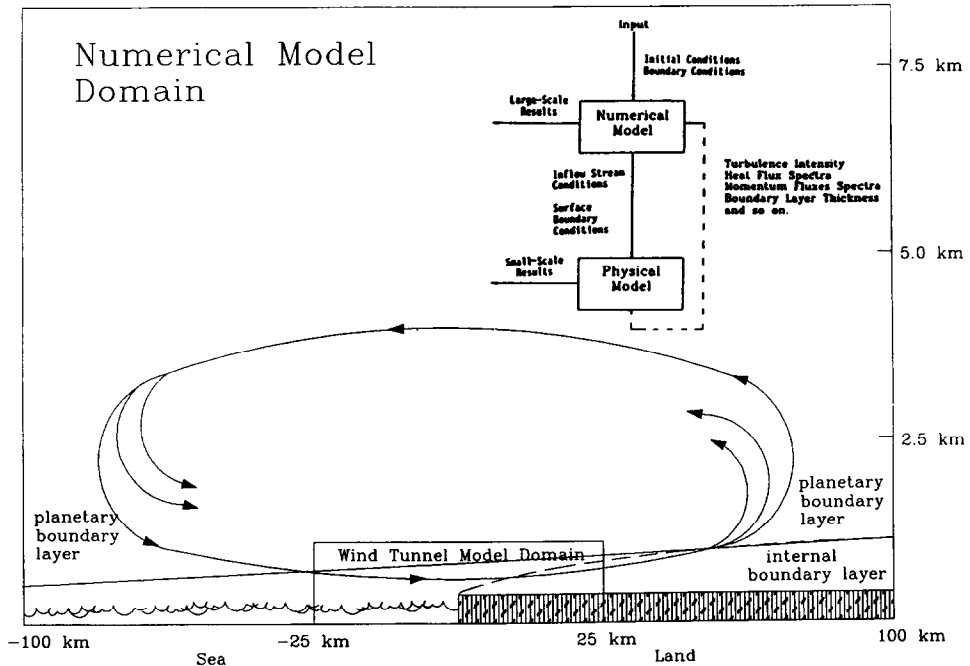


Fig. 14. Schematic showing wind-tunnel simulation domain embedded within a numerical model domain for a sea breeze. The inset is a conceptual flow diagram for the organization of the hybrid numerical-physical flow modeling system.

the time evolution of the larger-scale SLB circulation, which can then be used to drive wind-tunnel simulations of the near-surface flow during shorter, quasi-stationary periods. Thus, one can obtain some details about the local time evolution of marine flows from a conventional, steady-state, boundary-layer wind tunnel. This is somewhat analogous to a one-way, parasitic grid nest in a numerical model. Figure 14 illustrates this numerical-model/wind-tunnel nesting schematically. The inset flow chart outlines a supportive relationship between numerical and physical models. The numerical model provides a realistic time-dependent air-flow simulation over the larger mesoscale domain. The meteorological wind tunnel provides a realistic simulation at smaller scales not normally resolved by numerical models but is not able to model the full SLB circulation. Use of these two approaches together yields a hybrid method to simulate all scales of coastal marine flows.

5. Summary and Conclusions

This paper has examined the characteristics, capabilities, and limitations of two very different approaches for simulating atmospheric behavior on the mesoscale. Mesoscale numerical models solve a mathematical system of conservation equations formulated to describe atmospheric phenomena. They are a flexible, powerful tool but are limited by their mathematical descriptions and parameterizations of physical processes, by numerical errors associated with the solution techniques, and by computer power (which limits grid resolution and domain size). They also simulate ensemble-mean flows in most cases rather than flow realizations. Meteorological wind tunnels are, in effect, analog computers with 'near-infinite-simal' resolution and 'near-infinite' memory (Snyder, 1972). They employ real fluids, not mathematical models of fluids, and produce inherently viscous, turbulent, nonhydrostatic, non-Boussinesq, and compressible flows with no-slip boundary conditions. However, flows in scaled physical models can at best be only partially similar to their atmospheric prototype and cannot at present include all processes present in the atmosphere such as Coriolis acceleration, exchange of energy by radiation, and phase changes of water.

To date there has been little direct interaction between numerical modelers and wind-tunnel modelers. One reason for this lack of interaction is the difficulty in placing these two modeling approaches within the same conceptual framework. For instance, wind-tunnel models are scaled models with fixed physical dimensions, including model domain size, but a variable length-scale ratio. Numerical models, on the other hand, are full-scale models (LSR fixed and equal to 1) with a variable grid spacing and domain size. The operating range figures presented in this paper (Figures 9, 11, 12, and 13) are an attempt to provide a common basis for comparison. They have been constructed with the understanding that the model simulation grid and the model measurement grid may or may not be the same.

In a finite-difference numerical model, the governing equations are solved on a

discrete lattice of grid points, the simulation grid. Since values of various flow variables are available at each point of the simulation grid, the simulation grid is also the model measurement grid. In the wind tunnel, there is no need for a simulation grid. The real fluid in the scaled model obeys the exact laws of physics perfectly with no roundoff errors, phase errors, aliasing, or artificial damping, although with only partial similarity. Unlike the numerical model, the resolution of the wind-tunnel measurement grid in no way affects the accuracy of the flow solution (although the presence of an instrument probe may cause minor flow distortions). Moreover, in the wind tunnel the geometry of the sampling grid can vary greatly depending upon the sampling strategy. But it is the resolution of the measurement grid which limits our understanding of the modeled flow. Measurement grid resolution is thus a common aspect of both approaches. This concept might become clearer if we note that in spectral or pseudospectral numerical models, the simulation grid corresponds to a discrete lattice in wavenumber space while the measurement grid in physical space is a separate entity which can be specified independently of the simulation grid, although its resolution is still limited by that of the simulation grid.

Figures 9 and 11 show the OR's of mesoscale numerical models and meteorological wind tunnels in terms of model measurement resolution and atmospheric resolution. These OR's were determined based on a consideration of both fundamental model limitations, which are independent of the atmospheric phenomenon being modeled, and additional constraints imposed by the nature of the atmospheric phenomenon itself, including both forcing and response. Thus, these OR's would likely have to be modified if another atmospheric circulation system were to be investigated.

Figure 13 indicates that there is an OR common to both mesoscale numerical models and meteorological wind tunnels for the simulation of SLB's as well as simulation regimes in which only one of the two approaches would be suitable. It would appear then that these two approaches are complementary, suggesting a role for hybrid modeling. The common OR includes the coastal transition zone and thermal internal boundary layer. This aspect of SLB circulations can then be studied using both techniques, with a numerical model providing appropriate boundary conditions for the wind tunnel, and the wind-tunnel results providing evaluation data for the numerical model simulation and parameterizations (Figure 14).

Finally, the OR's presented in this paper were derived on the basis of present-day computer and wind-tunnel capabilities. It is likely that the OR's for both modeling approaches will expand as better facilities come online. In the case of computers, new semiconductor technologies and recent advances in parallel processing, both hardware and software, suggest continued improvements in computer power and hence in numerical model resolution and sophistication. In the case of meteorological wind tunnels, improvements in instrument technology should increase the number of measurements as well as their accuracy and spatial

resolution in both present facilities and in larger facilities with wider performance envelopes which may be constructed in the future.

Acknowledgements

The authors have benefited greatly from the word processing skills of Dallas McDonald and Tony Smith, who shepherded this paper through numerous revisions, and from the drafting ability of Judy Sorbie and AutoCAD expertise of Chris Duke. This work was supported by the Office of Naval Research under Contract N00014-88-K-0029.

References

- Abbs, D. J.: 1986, 'Sea-Breeze Interactions Along a Concave Coastline in Southern Australia: Observations and Numerical Modeling Study', *Mon. Wea. Rev.* **114**, 831-848.
- Anthes, R. A.: 1983, 'Regional Models of the Atmosphere in Middle Latitudes', *Mon. Wea. Rev.* **111**, 1306-1335.
- Anthes, R. A. and Warner, T. T.: 1978, 'Development of Hydrodynamic Models Suitable for Air Pollution and Other Mesometeorological Studies', *Mon. Wea. Rev.* **106**, 1045-1078.
- Armitt, J. and Counihan, J.: 1968, 'The Simulation of the Atmospheric Boundary Layer in a Wind Tunnel', *Atmos. Environ.* **2**, 49-71.
- Arritt, R. W.: 1987, 'The Effect of Water Surface Temperature on Lake Breezes and Thermal Internal Boundary Layers', *Boundary-Layer Meteorol.* **40**, 101-125.
- Arritt, R. W.: 1989, 'Numerical Modeling of the Offshore Extent of Sea Breezes', *Quart. J. Roy. Meteorol. Soc.* **115**, 547-570.
- Asai, T. and Mitsumoto, S.: 1978, 'Effects of an Inclined Land Surface on the Land and Sea Breeze Circulation: A Numerical Experiment', *J. Meteorol. Soc. Japan* **56**, 559-570.
- Atkinson, B. W.: 1981, *Meso-Scale Atmospheric Circulations*, Academic Press, New York, 495 pp.
- Avisar, R. and Pielke, R. A.: 1989, 'A Parameterization of Heterogeneous Land Surfaces for Atmospheric Numerical Models and Its Impact on Regional Meteorology', *Mon. Wea. Rev.* **117**, 2113-2136.
- Batchelor, G. K.: 1953, 'The Conditions for Dynamical Similarity of Motions of a Frictionless Perfect-Gas Atmosphere', *Quart. J. Roy. Meteorol. Soc.* **79**, 224-235.
- Blackadar, A. K.: 1977, 'High-Resolution Models of the Planetary Boundary Layer', in Pfaffin and Ziegler (eds.), *Advances in Environmental Science & Engineering*, Vol. 1, Gordon & Breach Science Publishers, pp. 50-85.
- Bornstein, R., Pechinger, U., Miller, R., Klotz, S., and Street, R.: 1987, 'Modeling the Polluted Coastal Urban Environment. Volume 1: The PBL Model', EPRI Final Report No. EA-5091, February, Electric Power Research Institute, Palo Alto, 161 pp. + App.
- Bougeault, P.: 1987, 'A Qualification Study of the French Weather Service Limited-Area Model', *Extended Abstracts Third AMS Conf. on Mesoscale Processes*, American Meteorological Society, Boston, pp. 51-52.
- Bradbury, L. J. S. and Castro, I. P.: 1971, 'A Pulsed-Wire Technique for Velocity Measurements in Highly Turbulent Flow', *J. Fluid Mech.* **49**, 657-691.
- Briatore, L., Elisei, G., and Longhetto, A.: 1980, 'Local Air Circulations over a Complex Coastal Site: A Comparison Among Field Surveys, Hydraulic- and Mathematical-Model Data', *Il Nuovo Cimento* **3C**, 365-381.
- Carpenter, K. M.: 1979, 'An Experimental Forecast Using a Non-Hydrostatic Mesoscale Model', *Quart. J. Roy. Meteorol. Soc.* **105**, 629-655.
- Carpenter, K. M. and Lowther, L. W.: 1982, 'An Experiment on the Initial Conditions for a Mesoscale Forecast', *Quart. J. Roy. Meteorol. Soc.* **108**, 643-660.
- Cermak, J. E.: 1971, 'Laboratory Simulation of the Atmospheric Boundary Layer', *AIAA Journal* **9**, 1746-1754.

- Cermak, J. E.: 1975, 'Applications of Fluid Mechanics to Wind Engineering – A Freeman Scholar Lecture', *J. Fluids Eng.* **97**, 9–38.
- Cermak, J. E.: 1982, 'Physical Modeling of the Atmospheric Boundary Layer in a Long Boundary-Layer Wind Tunnel', in T. A. Reinhold (ed.), *Wind Tunnel Modeling for Civil Engineering Application*, Cambridge University Press, pp. 97–125.
- Cermak, J. E., Sandborn, V. A., Plate, E. J., Binder, G. H., Chuang, H., Meroney, R. N., and Ito, S.: 1966, 'Simulation of Atmospheric Motion by Wind-Tunnel Flows', Report No. CER66-SI17, May, Department of Civil Engineering, Colorado State University, 101 pp. [Available from R. N. Meroney].
- Clark, T. L. and Farley, R. D.: 1984, 'Severe Downslope Windstorm Calculations in Two and Three Spatial Dimensions Using Anelastic Interactive Grid Nesting: A Possible Mechanism for Gustiness', *J. Atmos. Sci.* **41**, 329–350.
- Cotton, W. R.: 1986, 'Averaging and the Parameterization of Physical Processes in Mesoscale Models', in P. S. Ray (ed.), *Mesoscale Meteorology and Forecasting*, American Meteorological Society, Boston, pp. 614–635.
- Cotton, W. R. and Tripoli, G. J.: 1978, 'Cumulus Convection in Shear Flow – Three-Dimensional Numerical Experiments', *J. Atmos. Sci.* **35**, 1503–1521.
- Cotton, W. R. and Anthes, R. A.: 1989, *Storm and Cloud Dynamics*, Academic Press, New York, 883 pp.
- Crapper, P. F. and Linden, P. F.: 1974, 'The Structure of Turbulent Density Interfaces', *J. Fluid Mech.* **65**, 45–63.
- Dalu, G. A. and Cima, A.: 1983, 'Three-Dimensional Air Flow Over Sardinia', *Il Nuova Cimenta* **6**, 453–472.
- Dalu, G. A. and Pielke, R. A.: 1989, 'An Analytical Study of the Sea Breeze', *J. Atmos. Sci.* **46**, 1815–1825.
- Deardorff, J. W.: 1978, 'Efficient Prediction of Ground Surface Temperature and Moisture, with Inclusion of a Layer of Vegetation', *J. Geophys. Res.* **83**, 1889–1903.
- Defant, F.: 1950, 'Theorie der Land- und Seewinde', *Arch. Met. Geophys. Bioklim.* **A2**, 404–425.
- Durand, P., Brière, S., and Druilhet, A.: 1989, 'A Sea-Land Transition Observed during the COAST Experiment', *J. Atmos. Sci.* **46**, 96–116.
- Durrant, D. R.: 1989, 'Improving the Anelastic Approximation', *J. Atmos. Sci.* **46**, 1453–1461.
- Estoque, M. A.: 1961, 'A Theoretical Investigation of the Sea Breeze', *Quart. J. Roy. Meteorol. Soc.* **87**, 136–146.
- Estoque, M. A.: 1962, 'The Sea Breeze as a Function of the Prevailing Synoptic Situation', *J. Atmos. Sci.* **19**, 244–250.
- Estoque, M. and Gross, J. M.: 1981, 'Further Studies of a Lake Breeze. Part II: Theoretical Study', *Mon. Wea. Rev.* **109**, 619–634.
- Findlater, J.: 1964, 'The Sea Breeze and Inland Convection – An Example of Their Interrelation', *Meteorol. Mag.* **92**, 82–89.
- Fisher, E. L.: 1961, 'A Theoretical Study of the Sea Breeze', *J. Meteorol.* **18**, 216–233.
- Fosberg, M. A. and Schroeder, M. J.: 1966, 'Marine Air Penetration in Central California', *J. Appl. Meteorol.* **5**, 573–589.
- Garratt, J. R. and Physick, W. L.: 1985, 'The Inland Boundary Layer at Low Latitudes: II. Sea-Breeze Influences', *Boundary-Layer Meteorol.* **33**, 209–231.
- Garstang, M., Pielke, R. A. and Snow, J. W.: 1980a, 'Coastal Zone Wind Energy, Part II: Validation of the Coastal Zone Wind Power Potential, a Summary of the Field Experiment', U.S. Department of Energy Report PNL-3904, 43 pp. (Available from R. A. Pielke).
- Garstang, M., Pielke, R. A. and Snow, J. W.: 1980b, 'A Comparison of Model Predicted to Observed Winds in the Coastal Zone', U.S. Department of Energy Report PNL-3714, 73 pp. (Available from R. A. Pielke).
- Gottlieb, D. and Orszag, S. A.: 1977, *Numerical Analysis of Spectral Methods*, Society for Industrial and Applied Mathematics, Philadelphia, 172 pp.
- Hadfield, M. G.: 1988, 'The Response of the Atmospheric Convective Boundary Layer to Surface Inhomogeneities', Dept. of Atmospheric Science Paper No. 433, Colorado State University, Fort Collins, Colorado, U.S.A., 401 pp.

- Haltiner, G. J. and Williams, R. T.: 1980, *Numerical Prediction and Dynamic Meteorology*, Second Edition, John Wiley and Sons, New York, 477 pp.
- Haurwitz, B.: 1947, 'Comments on the Sea-Breeze Circulation', *J. Meteorol.* **4**, 1913-1917.
- Helmis, C. G., Asimakopoulou, D. N., Deligiorgi, D. G., and Lalas, D. P.: 1987, 'Observations of Sea-Breeze Fronts near the Shoreline', *Boundary-Layer Meteorol.* **38**, 395-410.
- Hinze, J. O.: 1975, *Turbulence, 2nd Ed.*, McGraw-Hill, New York, 790 pp.
- Hjelmfelt, M. R. and Braham, Jr., R. R.: 1983, 'Numerical Simulation of the Airflow over Lake Michigan for a Major Lake-Effect Snow Event', *Mon. Wea. Rev.* **111**, 205-219.
- Hsu, H.-M.: 1979, 'Numerical Simulations of Mesoscale Precipitation Systems', Ph.D. Dissertation, Dept. of Atmospheric and Oceanic Science, University of Michigan, Ann Arbor, Michigan, 342 pp.
- Itoh, H. and Sugimara, H.: 1989, 'Numerical Experiments on the Interaction of Ocean and Bay Breezes', *J. Meteorol. Soc. Japan* **67**, 411-428.
- Jeffreys, H.: 1922, 'On the Dynamics of Wind', *Quart. J. Roy. Meteorol. Soc.* **48**, 29-47.
- Kikuchi, Y., Arakawa, S., Kimura, F., Shirasaki, K., and Nagano, Y.: 1981, 'Numerical Study on the Effects of Mountains on the Land and Sea Breeze Circulation in the Kanto District', *J. Meteorol. Soc. Japan* **59**, 723-738.
- Kimura, F.: 1985, 'A Numerical Simulation of Local Winds and Photochemical Air Pollution (II): Application to the Kanto Plain', *J. Meteorol. Soc. Japan* **63**, 923-935.
- Kimura, R. and Eguchi, T.: 1978, 'On Dynamical Processes of Sea- and Land-Breeze Circulation', *J. Meteorol. Soc. Japan* **56**, 67-85.
- Kitada, T., Carmichael, G. R., and Peters, L. K.: 1984, 'Numerical Simulation of the Transport of Chemically Reactive Species under Land- and Sea-Breeze Circulations', *J. Climate Appl. Meteorol.* **23**, 1153-1172.
- Klemp, J. B. and Wilhelmson, R. B.: 1978, 'The Simulation of Three-Dimensional Convective Storm Dynamics', *J. Atmos. Sci.* **35**, 1070-1096.
- Kozo, T. L.: 1982, 'An Observational Study of Sea Breezes Along the Alaskan Beaufort Sea Coast. Part I', *J. Appl. Meteorol.* **21**, 891-905.
- Kusuda, M. and Alpert, P.: 1983, 'Anti-Clockwise Rotation of the Wind Hodograph. Part I: Theoretical Study', *J. Atmos. Sci.* **40**, 487-499.
- Li, W. W. and Meroney, R. N.: 1985, 'The Estimation of Atmospheric Dispersion at Nuclear Reactor Plants Utilizing Real Time Anemometer Statistics', Report No. NUREG/CR-4072, January, U.S. Nuclear Regulatory Commission, Washington, D.C., 244 pp.
- Long, P. E., Jr. and Pepper, D. W.: 1981, 'An Examination of Some Simple Numerical Schemes for Calculating Scalar Advection', *J. Appl. Meteorol.* **20**, 146-156.
- Lumley, J. L. and Panofsky, H. A.: 1964, *The Structure of Atmospheric Turbulence*, Interscience, New York, 239 pp.
- Lyons, W. A.: 1972, 'The Climatology and Prediction of the Chicago Lake Breeze', *J. Appl. Meteorol.* **11**, 1259-1270.
- Lyons, W. A., Schuh, J. A., and McCumber, M.: 1979, 'Comparison of Observed Mesoscale Lake Breeze Wind Fields to Computations Using the University of Virginia Mesoscale Model', *Proc. Fourth AMS Symp. on Turbulence, Diffusion, and Air Pollution*, Jan. 15-18, Reno, Nevada, American Meteorological Society, Boston, pp. 572-575.
- Mahfouf, J. F., Richard, E., Mascart, P., Nickerson, E. C., and Rosset, R.: 1987, 'A Comparative Study of Various Parameterizations of the Planetary Boundary Layer in a Numerical Mesoscale Model', *J. Climate Appl. Meteorol.* **26**, 1671-1695.
- Mahrer, Y. and Pielke, R. A.: 1976, 'Numerical Simulation of the Airflow Over Barbados', *Mon. Wea. Rev.* **104**, 1392-1402.
- Mahrer, Y. and Pielke, R. A.: 1977, 'The Effects of Topography on Sea and Land Breezes in a Two-Dimensional Numerical Model', *Mon. Wea. Rev.* **105**, 1151-1162.
- Mak, M. K. and Walsh, J. E.: 1976, 'On the Relative Intensities of Sea and Land Breezes', *J. Atmos. Sci.* **33**, 242-251.
- Martin, C. L. and Pielke, R. A.: 1983, 'The Adequacy of the Hydrostatic Assumption in Sea Breeze Modeling Over Flat Terrain', *J. Atmos. Sci.* **40**, 1472-1481.
- McCumber, M. C. and Pielke, R. A.: 1981, 'Simulation of the Effects of Surface Fluxes of Heat and Moisture in a Mesoscale Numerical Model. I. Soil Layer', *J. Geophys. Res.* **86**, 9929-9938.

- McNider, R. T., Mizzi, A. P. and Pielke, R. A.: 1982, 'Numerical Investigation of Low Level Jets in Coastal Zones', *Proc. First Int'l Conf. on Meteorological and Air/Sea Interaction of the Coastal Zone*, The Hague, Netherlands, 10-14 May 1982, American Meteorological Society, Boston, pp. 190-195.
- McNider, R. T. and Pielke, R. A.: 1984, 'Numerical Simulation of Slope and Mountain Flows', *J. Climate Appl. Meteorol.* **23**, 1441-1453.
- McPherson, R. D.: 1970, 'A Numerical Study of the Effect of a Coastal Irregularity on the Sea Breeze', *J. Appl. Meteorol.* **9**, 767-777.
- Merilees, P. E. and Orszag, S. A.: 1979, 'The Pseudospectral Method', *Numerical Methods Used In Atmospheric Models, Vol. II*, GARP Publ. Ser. No. 17, September, World Meteorological Organization, Geneva, pp. 276-299. (Available from Secretariat of the World Meteorological Organization, Case Postale no. 5, CH-1211, Geneva 20, Switzerland).
- Meroney, R. N.: 1981, 'Physical Simulation of Dispersion in Complex Terrain and Valley Drainage Flow Situations', *Air Pollution Modelling and Its Application I*, Plenum Press, New York, pp. 489-508.
- Meroney, R. N.: 1986, 'Guidelines for Fluid Modeling of Liquefied Natural Gas Cloud Dispersion. Vol. II: Technical Support Document', Report No. GRI 86/0102.2, May, Gas Research Institute, Chicago, Illinois, 263 pp.
- Meroney, R. N.: 1987, 'Guidelines for Fluid Modeling of Dense Gas Cloud Dispersion', *J. Hazard. Mater.* **17**, 23-46.
- Meroney, R. N., Cermak, J. E. and Yang, B. T.: 1975a, 'Modeling of Atmospheric Transport and Fumigation at Shoreline Sites', *Boundary-Layer Meteorol.* **9**, 69-90.
- Meroney, R. N., Cermak, J. E., Hill, D., and Garrison, J. A.: 1975b, 'Wind-Tunnel Model Study of Diffusion - Coalplex Project, A.E. and C.I. Limited, South Africa', July, Report No. CER75-76RNM-JEC-JAG3, Department of Civil Engineering, Colorado State University, Fort Collins, 105 pp.
- Meroney, R. N., Sandborn, V. A., Bouwmeester, R. J. B., Chien, H. C., and Rider, M.: 1978, 'Sites for Wind Power Installation: Physical Modeling of the Influence of Hills, Ridges and Complex Terrain on Wind Speed and Turbulence, Parts I, II, and III', D.O.E. Report No. RLO/2438-7/3, U.S. Department of Energy, 175 pp.
- Méry, P., Schon, J.-P., and Solal, J.: 1974, 'Comparison of Thermally Neutral and Unstable Shear Flows in the Wind Tunnel and the Atmosphere', *Adv. Geophys.* **18B**, 273-287.
- Mesinger, F. and Arakawa, A.: 1976, 'Numerical Methods Used in Atmospheric Models', Vol. 1, *GARP Publ. Ser. No. 17*, August, World Meteorological Organization, Geneva, 64 pp. (Available from Secretariat of the World Meteorological Organization, Case Postale no. 5, CH-1211, Geneva 20, Switzerland).
- Mitsumoto, S., Ueda, H., and Ozoe, H.: 1983, 'A Laboratory Experiment on the Dynamics of the Land and Sea Breeze', *J. Atmos. Sci.* **40**, 1228-1240.
- Neff, D. E. and Meroney, R. N.: 1982, 'The Behavior of LNG Vapor Clouds: Wind-Tunnel Tests on the Modeling of Heavy Plume Dispersion', Report No. GRI 80/0145, Gas Research Institute, Chicago, Illinois, 120 pp.
- Neumann, J.: 1973, 'Sea and Land Breezes in the Classical Greek Literature', *Bull. Amer. Meteorol. Soc.* **54**, 5-8.
- Neumann, J.: 1977, 'On the Rotation Rate of the Direction of Sea and Land Breezes', *J. Atmos. Sci.* **34**, 1913-1917.
- Neumann, J.: 1984, 'The Coriolis Force in Relation to the Sea and Land Breezes - A Historical Note', *Bull. Amer. Meteorol. Soc.* **65**, 24-26.
- Neumann, J. and Mahrer, Y.: 1971, 'A Theoretical Study of the Land and Sea Breeze Circulation', *J. Atmos. Sci.* **28**, 532-542.
- Neumann, J. and Mahrer, Y.: 1973, 'Evolution of a Sea Breeze Front: A Numerical Study', *Climatological Research, The Hermann Flohn 60th Birthday Volume*, Meteorological Institute, University of Bonn, West Germany, pp. 481-492.
- Neumann, J. and Mahrer, Y.: 1974, 'A Theoretical Study of the Sea and Land Breezes of Circular Islands', *J. Atmos. Sci.* **31**, 2027-2039.
- Niino, H.: 1987, 'The Linear Theory of Land and Sea Breeze Circulation', *J. Meteor. Soc. Japan* **65**, 901-921.
- Noonan, J. A. and Smith, R. K.: 1986, 'Sea-Breeze Circulations over Cape York Peninsula and the Generation of Gulf of Carpentaria Cloud Line Disturbances', *J. Atmos. Sci.* **43**, 1679-1693.

- Noonan, J. A. and Smith, R. K.: 1987, 'The Generation of North Australian Cloud Lines and the Morning Glory', *Aust. Meteorol. Mag.* **35**, 31–45.
- Ogawa, Y., Griffiths, R., and Hoydysh, W. G.: 1975, 'A Wind-Tunnel Study of Sea Breeze Effects', *Boundary-Layer Meteorol.* **8**, 141–161.
- Ogawa, Y., Diosey, P. G., Uehara, K., and Ueda, H.: 1981, 'A Wind Tunnel for Studying the Effects of Thermal Stratification in the Atmosphere', *Atmos. Environ.* **15**, 807–821.
- Ogawa, Y., Diosey, P. G., Uehara, K., and Ueda, H.: 1985, 'Wind Tunnel Observation of Flow and Diffusion under Stable Stratification', *Atmos. Environ.* **19**, 65–74.
- Ogura, Y. and Phillips, N. A.: 1962, 'Scale Analysis of Deep and Shallow Convection in the Atmosphere', *J. Atmos. Sci.* **19**, 173–179.
- Olfe, D. B. and Lee, R. L.: 1971, 'Linearized Calculations of Urban Heat Island Convection Effects', *J. Atmos. Sci.* **28**, 1374–1388.
- Orgill, M. M.: 1971, 'Laboratory Simulation and Field Estimates of Atmospheric Transport-Dispersion over Mountainous Terrain', Ph.D. Dissertation, Colorado State University, Fort Collins, 302 pp.
- Orlanski, I.: 1975, 'A Rational Subdivision of Scales for Atmospheric Processes', *Bull. Amer. Meteorol. Soc.* **56**, 527–530.
- Pearce, R. P.: 1955, 'The Calculation of a Sea-Breeze Circulation in Terms of the Differential Heating Across the Coastline', *Quart. J. Roy. Meteorol. Soc.* **81**, 351–381.
- Pearson, R. A.: 1975, 'On the Asymmetry of the Land-Breeze/Sea-Breeze Circulation', *Quart. J. Roy. Meteorol. Soc.* **101**, 529–536.
- Pepper, D. W., Kern, C. D., and Long, Jr., P. E.: 1979, 'Modeling the Dispersion of Atmospheric Pollution Using Cubic Splines and Chapeau Functions', *Atmos. Environ.* **13**, 223–237.
- Physick, W.: 1976, 'A Numerical Model of the Sea-Breeze Phenomenon over a Lake or Gulf', *J. Atmos. Sci.* **33**, 2107–2135.
- Physick, W. L.: 1980, 'Numerical Experiments on the Inland Penetration of the Sea Breeze', *Quart. J. Roy. Meteorol. Soc.* **106**, 735–746.
- Physick, W. L. and Smith, R. K.: 1985, 'Observations and Dynamics of Sea-Breezes in Northern Australia', *Aust. Meteorol. Mag.* **33**, 51–63.
- Pielke, R. A.: 1974a, 'A Three-Dimensional Numerical Model of the Sea Breezes Over South Florida', *Mon. Wea. Rev.* **102**, 115–139.
- Pielke, R. A.: 1974b, 'A Comparison of Three-Dimensional and Two-Dimensional Numerical Predictions of Sea Breezes', *J. Atmos. Sci.* **31**, 1577–1585.
- Pielke, R. A.: 1982, 'The Role of Mesoscale Numerical Models in Very-Short-Range Forecasting', in K. Browning (ed.), *Nowcasting*, Academic Press, New York, pp. 207–221.
- Pielke, R. A.: 1984, *Mesoscale Meteorological Modeling*, Academic Press, New York, 612 pp.
- Pielke, R. A.: 1987, 'The Challenge of Using Mesoscale Data in Mesoscale Models', *Proc. Symposium on Mesoscale Analysis and Forecasting, Incorporating Nowcasting*, ESA SP-282, August 17–19, 1987, Vancouver, British Columbia, Canada, European Space Agency, Paris, pp. 651–652.
- Pielke, R. A. and Mahrer, Y.: 1978, 'Verification Analysis of the University of Virginia Three-Dimensional Mesoscale Model Prediction over South Florida for 1 July 1973', *Mon. Wea. Rev.* **106**, 1568–1589.
- Pielke, R. A., McNider, R. T., Segal, M., and Mahrer, Y.: 1983, 'The Use of a Mesoscale Numerical Model for Evaluations of Pollutant Transport and Diffusion in Coastal Regions and over Irregular Terrain', *Bull. Amer. Meteorol. Soc.* **64**, 243–249.
- Pielke, R. A. and Segal, M.: 1986, 'Mesoscale Circulations Forced by Differential Terrain Heating', in P. S. Ray (ed.), *Mesoscale Meteorology and Forecasting*, American Meteorological Society, Boston, pp. 516–548.
- Pierson, W. J.: 1950, 'The Effects of Eddy Viscosity, Coriolis Deflection and Temperature Fluctuation on the Sea Breeze as a Function of Time and Height', *Meteor. Pap.*, No. 1, College of Engineering, New York University, 30 pp.
- Purser, R. J.: 1987, 'The Filtering of Meteorological Fields', *J. Climate Appl. Meteorol.* **26**, 1764–1769.
- Puttock, J. S. and Colenbrander, G. W.: 1985, 'Dense Gas Dispersion – Experimental Research', in R. V. Portelli (ed.), *Proc. Heavy Gas (LNG/LPG) Workshop*, Jan. 29–30, Toronto, Ontario, pp. 32–50. (Available from Concord Scientific Corporation, 2 Tippet Rd., Downsview, Ontario, Canada, M3H 2V2).
- Raymond, W. H.: 1988, 'High-Order Low-Pass Implicit Tangent Filters for Use in Finite Area Calculations', *Mon. Wea. Rev.* **116**, 2132–2141.

- Rood, R. B.: 1987, 'Numerical Advection Algorithms and Their Role in Atmospheric Transport and Chemistry Models', *Rev. Geophys.* **25**, 71–100.
- Rotunno, R.: 1983, 'On the Linear Theory of the Land and Sea Breeze', *J. Atmos. Sci.* **40**, 1999–2009.
- Schmidt, F. H.: 1947, 'An Elementary Theory of the Land- and Sea-Breeze Circulation', *J. Meteorol.* **4**, 9–15.
- Schroeder, M. J., Fosberg, M. A., Creamer, O. P. and O'Dell, C. A.: 1967, 'Marine Air Invasion of the Pacific Coast: A Problem Analysis', *Bull. Amer. Meteorol. Soc.* **48**, 802–808.
- Segal, M., McNider, R. T., Pielke, R. A., and McDougal, D. S.: 1982a, 'A Numerical Model Simulation of the Regional Air Pollution Meteorology of the Greater Chesapeake Bay Area – Summer Day Case Study', *Atmos. Environ.* **16**, 1381–1397.
- Segal, M., Mahrer, Y., and Pielke, R. A.: 1982b, 'Application of a Numerical Mesoscale Model for the Evaluation of Seasonal Persistent Regional Climatological Patterns', *J. Appl. Meteorol.* **21**, 1754–1762.
- Segal, M., Purdom, J. F. W., Song, J. L., Pielke, R. A., and Mahrer, Y.: 1986, 'Evaluation of Cloud Shading Effects on the Generation and Modification of Mesoscale Circulations', *Mon. Wea. Rev.* **114**, 1201–1212.
- Segal, M., Avissar, R., McCumber, M. C., and Pielke, R. A.: 1988a, 'Evaluation of Vegetation Effects on the Generation and Modification of Mesoscale Circulations', *J. Atmos. Sci.* **45**, 2268–2292.
- Segal, M., Pielke, R. A., Arritt, R. W., Moran, M. D., Yu, C.-H., and Henderson, D.: 1988b, 'Application of a Mesoscale Atmospheric Dispersion Modeling System to the Estimation of SO₂ Concentrations from Major Elevated Point Sources in Southern Florida', *Atmos. Environ.* **22**, 1319–1334.
- SethuRaman, S. and Cermak, J. E.: 1974, 'Physical Modeling of Flow and Diffusion over an Urban Heat Island', *Adv. Geophys.* **18B**, 223–240.
- SethuRaman, S. and Cermak, J. E.: 1975, 'Mean Temperature and Mean Concentration Distributions over a Physically Modelled Three-Dimensional Heat Island for Different Stability Conditions', *Boundary-Layer Meteorol.* **9**, 427–440.
- Simpson, J. E.: 1967, 'Aerial and Radar Observations of Some Sea-Breeze Fronts', *Weather* **22**, 306–317.
- Simpson, J. E.: 1969, 'A Comparison between Laboratory and Atmospheric Density Currents', *Quart. J. Roy. Meteorol. Soc.* **95**, 758–765.
- Simpson, J. E.: 1987, *Gravity Currents In the Environment and the Laboratory*, Ellis Horwood Ltd., Chichester, 244 pp.
- Simpson, J. E., Mansfield, D. A., and Milford, J. R.: 1977, 'Inland Penetration of Sea-Breeze Fronts', *Quart. J. Roy. Meteorol. Soc.* **103**, 47–76.
- Simpson, J. E. and Britter, R. E.: 1979, 'The Dynamics of a Head of a Gravity Current Advancing over a Horizontal Surface', *J. Fluid Mech.* **94**, 477–495.
- Simpson, J. E. and Britter, R. E.: 1980, 'A Laboratory Model of an Atmospheric Mesofront', *Quart. J. Roy. Meteorol. Soc.* **106**, 485–500.
- Smith, R. B.: 1979, 'The Influence of Mountains on the Atmosphere', *Adv. Geophys.* **21**, 87–230.
- Snyder, W. H.: 1972, 'Similarity Criteria for the Application of Fluid Models to the Study of Air Pollution Meteorology', *Boundary-Layer Meteorol.* **3**, 113–134.
- Stephens, G. L.: 1984, 'The Parameterization of Radiation for Numerical Weather Prediction and Climate Models', *Mon. Wea. Rev.* **112**, 826–867.
- Steyn, D. G. and Ayyotte, K. W.: 1985, 'Application of Two-Dimensional Terrain Height Spectra to Mesoscale Modeling', *J. Atmos. Sci.* **42**, 2884–2887.
- Steyn, D. G. and McKendry, I. G.: 1988, 'Quantitative and Qualitative Evaluation of a Three-Dimensional Mesoscale Numerical Model Simulation of a Sea Breeze in Complex Terrain', *Mon. Wea. Rev.* **116**, 1914–1926.
- Stunder, M. and SethuRaman, S.: 1985, 'A Comparative Evaluation of the Coastal Internal Boundary-Layer Height Equations', *Boundary-Layer Meteorol.* **32**, 177–204.
- Sun, W.-Y. and Orlanski, I.: 1981a, 'Large Mesoscale Convection and Sea Breeze Circulation. Part I: Linear Stability Analysis', *J. Atmos. Sci.* **38**, 1675–1693.
- Sun, W.-Y. and Orlanski, I.: 1981b, 'Large Mesoscale Convection and Sea Breeze Circulation. Part II: Nonlinear Numerical Model', *J. Atmos. Sci.* **38**, 1694–1706.

- Sutton, O. G.: 1949, *Atmospheric Turbulence*, Methuen, London, 111 pp.
- Tapp, M. C. and White, P. W.: 1976, 'A Non-Hydrostatic Mesoscale Model', *Quart. J. Roy. Meteorol. Soc.* **102**, 277-296.
- Townsend, A. A.: 1956, *The Structure of Turbulent Shear Flow*, Cambridge University Press, 315 pp.
- Tremback, C. J., Powell, J., Cotton, W. R., and Pielke, R. A.: 1987, 'The Forward-in-Time Upstream Advection Scheme: Extension to Higher Orders', *Mon. Wea. Rev.* **115**, 540-555.
- Ueda, H.: 1983, 'Effects of External Parameters on the Flow Field in the Coastal Region - A Linear Model', *J. Climate Appl. Meteorol.* **22**, 312-321.
- Ukeguchi, N., Sakata, H., Okamoto, H., and Ide, Y.: 1967, 'Study of Stack Gas Diffusion', Tech. Bull. No. 52, August, Mitsubishi Heavy Industries, Ltd., Nagasaki, Japan, 13 pp.
- Ulrickson, B. L.: 1988, 'Mesoscale Circulations in the Los Angeles Basin: A Numerical Study', Ph.D. Dissertation, Dept. of Atmospheric Sciences, University of Washington, Seattle, Washington, 256 pp. (Available from University Microfilms, 300 North Zeeb Road, Ann Arbor, Michigan, 48106).
- Venkatram, A.: 1986, 'An Examination of Methods to Estimate the Height of the Coastal Internal Boundary Layer', *Boundary-Layer Meteorol.* **36**, 149-156.
- Wallington, C. E.: 1959, 'Structure of Sea Breeze Front as Revealed by Gliding Flights', *Weather* **14**, 263-269.
- Wallington, C. E.: 1961, 'An Introduction to the Sea Breeze Front', *Schweitz. Aero-Revue* **7**, 393-397.
- Wallington, C. E.: 1965, 'Gliding Through a Sea Breeze Front', *Weather* **20**, 140-143.
- Walsh, J. E.: 1974, 'Sea Breeze Theory and Applications', *J. Atmos. Sci.* **31**, 2012-2026.
- Warner, T. T., Anthes, R. A., and McNab, A. L.: 1978, 'Numerical Simulations with a Three-Dimensional Mesoscale Model', *Mon. Wea. Rev.* **106**, 1079-1099.
- Wyngaard, J. C.: 1982, 'Boundary-Layer Modeling', in F. T. M. Nieuwstadt and H. van Dop (eds.), *Atmospheric Turbulence and Air Pollution Modelling*, D. Reidel Publishing Co., Dordrecht, pp. 69-106.
- Yamada, T. and Meroney, R. N.: 1971, 'Numerical and Wind-Tunnel Simulation of Response of Stratified Shear Layers to Nonhomogeneous Surface Features', C.S.U. Dept. of Civil Engineering Report, CER70-711Y-RNM62, AD-730-953. (Available from R. N. Meroney).
- Yamada, T. and Meroney, R. N.: 1974, 'A Wind-Tunnel Facility for Simulating Mountain and Heated-Island Gravity Waves', *Boundary-Layer Meteorol.* **7**, 65-80.
- Yan, H. and Anthes, R. A.: 1987, 'The Effect of Latitude on the Sea Breeze', *Mon. Wea. Rev.* **115**, 936-956.
- Yan, H. and Anthes, R. A.: 1988, 'The Effect of Variations in Surface Moisture on Mesoscale Circulations', *Mon. Wea. Rev.* **116**, 192-208.
- Young, G. S. and Pielke, R. A.: 1983, 'Application of Terrain Height Variance Spectra to Mesoscale Modeling', *J. Atmos. Sci.* **40**, 2555-2560.
- Young, G. S., Pielke, R. A., and Kessler, R. C.: 1984, 'A Comparison of the Terrain Height Variance Spectra of the Front Range with that of a Hypothetical Mountain', *J. Atmos. Sci.* **41**, 1249-1250.
- Zhang, D.-L., Chang, H.-R., Seaman, N. L., Warner, T. T., and Fritsch, J. M.: 1986, 'A Two-Way Interactive Nesting Procedure with Variable Terrain Resolution', *Mon. Wea. Rev.* **114**, 1330-1339.
- Zhang, D.-L., Hsie, E.-Y., and Moncrieff, M. W.: 1988, 'A Comparison of Explicit and Implicit Predictions of Convective and Stratiform Precipitating Weather Systems with a Meso- β -scale Numerical Model', *Quart. J. Roy. Meteorol. Soc.* **114**, 31-60.